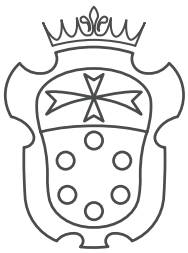

SCUOLA
NORMALE
SUPERIORE

Classe di Scienze

Corso di perfezionamento in
Matematica

XXXV ciclo

Fibering Hyperbolic Manifolds and Hyperbolic Groups

Settore Scientifico Disciplinare **MAT/03**

Candidato
Giovanni Italiano

Relatore

Prof. Bruno Martelli

Supervisione interna

Prof. Andrea Malchiodi

Anno accademico 2022–2023

Acknowledgements

First and foremost, I would like to express my deepest gratitude to my advisor, Bruno Martelli, for not only introducing me to this beautiful project but also for his support throughout this journey. His extensive knowledge, insightful feedback, and exceptional mentorship have been invaluable to me. The wisdom he shared, coupled with his patient guidance and encouragement, helped shape both my academic pursuits and personal growth. I am sincerely appreciative of his dedication and support, which greatly contributed to my journey in this field of study and provided me with a strong foundation for my future endeavors.

This journey would have been unimaginable without Matteo, a dear friend and an exceptionally talented colleague, who joined me in embracing this project. Collaborating with him over the years in Pisa has been not only a great pleasure but also an enriching experience. His unique insights, creativity, and dedication have significantly contributed to both the project and my personal growth. I feel incredibly fortunate to have had the opportunity to share this journey with him.

My heartfelt thanks go beyond what words can express to my dearest friends Clara and Nicola. Their unwavering encouragement and support were my pillars of strength during times when I felt discouraged, downhearted, and overwhelmed. They not only provided emotional support but also welcomed me into their home, offering their presence whenever loneliness seemed insurmountable. It was within the warmth and comfort of their home that the foundations of this thesis began to materialize. I would like to extend a special thank you to little Camilla, whose adorable ways and contagious joy provided a much-needed break from the intense focus on my thesis, reminding me of the simplicity and purity of happiness, even in the midst of complex challenges.

It is simply impossible to overstate the importance of the help I received from my parents throughout my life, and especially in this writing process. I extend my heartfelt gratitude to my mother, whose unwavering presence by my side during moments of struggle and doubt was a beacon of hope and resilience. Her steadfast support prevented me from giving in to surrender, providing the strength I needed to persevere. Similarly, I am profoundly grateful to my father, whose encouragement and guidance have been

fundamental in my thesis journey. I particularly thank him for proof-reading this thesis: his wise counsel and supportive words have been pivotal in polishing this work.

Additionally, a special note of thanks goes to my brothers and the entire family, whose constant encouragement and faith in me have been sources of comfort and strength. A final thanks goes to my brother Manfredi, whose assistance in verifying the coherence of some figures in my thesis was immensely helpful.

If it weren't for the invaluable help of all these individuals, I would likely still be struggling with composing the first chapter of this thesis, rather than searching for the right words to conclude these acknowledgements.

Thanks should also go to all the other PhD students in geometry and topology in Pisa, for the vibrant and intellectually stimulating environment they all contributed to create. Special thanks are owed to everyone who played a role in organizing the Baby Geometri seminars. Witnessing the growth and evolution of this project over the past years has brought me great satisfaction.

I'd like to acknowledge the entire community of Scuola Normale, where I never failed to find friends, mentors, and engaging conversations. These nine years in Pisa have been wonderful, thanks to the amazing people that surrounded me. I am particularly thankful to Federica and Adele, for their support in my moments of sadness and self-doubt.

I also extend my appreciation to my other friends in Pisa, Rome, and the rest of the world. The bonds we have shared and the support you have provided have been essential to me, and I hold a special place in my heart for each one of you.

Lastly, I wish to acknowledge the efforts of everyone involved in organizing the Mathematical Olympiads, both in Italy and globally. Their dedication and hard work ignited my passion for these subjects, and provided me with opportunities that have shaped my path. I earnestly hope that their efforts will continue to bear fruit, inspiring future generations of mathematicians to discover their calling as I have found mine.

Contents

Introduction

Hyperbolic geometry has long been acknowledged as pivotal in unraveling the intricate mysteries of the world of low-dimensional topology.

In the two-dimensional context, the Gauss-Bonnet Theorem shows that topology and geometry are closely intertwined. In particular, all closed surfaces admit a metric of constant curvature, and in all but a finite number of them this metric is hyperbolic. Three-dimensional topology is much more complicated, and has been one of the most active fields of research in the last century. The crucial step in advancing our knowledge on this topic has been Perel'man confirmation of Thurston's Geometrization Conjecture; every 3-dimensional manifold decomposes into geometric pieces, each modelled on one of eight geometries. Among these eight models, hyperbolic geometry stands out again as the most interesting, the most common, and the most mysterious.

As the dimension increases, the impact of hyperbolic geometry seems to fade away. Moreover, there is a significant lack of tools to even build and study concrete examples.

In our thesis, we construct some interesting examples of hyperbolic manifold in dimensions 4, 5, 6, 7 and 8, building up on some of the few tools available. This answers some long-standing open questions regarding hyperbolic groups.

One of the most fascinating phenomena in the topology of 3-manifolds is the existence of hyperbolic manifolds that fiber over the circle S^1. As pointed out by Thurston in [59], such fibrations are quite paradoxical, as the fiber is as far as possible from being geodesic. In fact, its preimage in $\mathbb{H}^3$ consists on the union of smooth disks that are at bounded distance from each other, but their limit set in the boundary of $\mathbb{H}^3$ is the whole sphere at infinity. In particular, the metric induced on the fiber is not hyperbolic.

The first example of a hyperbolic 3-manifold fibering over the circle was discovered by Jørgensen [32] in 1977. Since then, many contributions were given to the topic; helping to deepen our understanding of these manifolds. In particular, Thurston [58] characterized which fiber bundles over the circle S^1 admit a hyperbolic structure; and more recent contributions by Agol and Wise [1, 62] confirmed the *virtual fibering conjecture*: each closed hyperbolic 3-manifold admits a finite cover that is a fiber bundle over the circle.

Although the situation in dimension 3 is well understood, in dimension $n > 3$ no examples of fibering hyperbolic n-manifolds were known until [30]. Note that an even dimensional hyperbolic manifold M cannot fiber over S^1, due to an Euler characteristic obstruction. In fact, the Euler characteristic $\chi(M)$ of a fiber bundle over S^1 is always 0; but a generalization of the Gauss-Bonnet Theorem ensures that if M is hyperbolic, then $\chi(M)$ is proportional to the volume of M, and therefore cannot vanish.

To find a fibering hyperbolic n-manifold with $n > 3$, the first dimension to look at is therefore $n = 5$. The main theorem presented in this thesis is the following:

Theorem A: *There is a complete, hyperbolic manifold M^5 with finite volume which fibers over the circle S^1.*

The manifold M^5 is built using a construction of Vesnin [60], starting from a right-angled polytope P^5 and a colouring of its facets. The main technique used to build and study the fibration map $f\colon M^5 \to S^1$ is Bestvina-Brady theory [9], enriched with a combinatorial game by Jankiewicz, Norin and Wise [31]. With the use of these tools, we manage to translate a description of f into a combinatorial language, which interacts nicely with the starting construction. The exploitation of the extraordinary symmetries of the polytope P^5 contributes to simplify the needed computations.

Using similar techniques, we construct a manifold M^n for each dimension $n = 3, ..., 8$, and a map $f\colon M^n \to S^1$. These maps are algebraic fibrations, in the sense that the kernel of the induced map $f_*\colon \pi_1(M^n) \to \pi_1(S^1) = \mathbb{Z}$ is finitely generated.

In dimensions 3 and 5, the maps will be fibrations. In the 4-dimensional case, the map cannot be a fibration (since 4 is even), but it has the minimal possible number of critical points. In particular, it is the perfect circle-valued Morse function constructed in [6]. In dimension 7 and 8, we manage to promote the finitely generated kernel to be finitely presented.

When a hyperbolic 3-manifold M fibers over S^1, the fiber F is a finite type surface. As we have already mentioned, even if F can in principle carry a hyperbolic metric, the metric induced on F by the metric of M is not hyperbolic.

This incompatibility between the hyperbolic structure and the structure of a fiber bundle carries on in higher dimension $n \geq 5$, in an even more drastic way: the monodromy of the fiber F has infinite order in $\mathrm{Out}(\pi_1(F))$, so in particular F cannot admit *any* hyperbolic metric by Mostow Rigidity.

This leads us to turn our attention to hyperbolic groups. We say that a group is of *finite type* if it has a finite classifying space. With some technical precautions, due to the fact that the manifold M^5 is cusped (and hence not closed), we are able to use Theorem A to prove the following.

Theorem B: *There is a hyperbolic group G that contains a subgroup $H < G$ of finite type that is not hyperbolic.*

This theorem answers a well-known open question, raised by Bestvina [8, Question 1.1], Brady [15, Question 7.2], Bridson [12, Question 4.1], and Jankiewicz, Norin and Wise [31, Section 7]. A finitely generated subgroup of a hyperbolic group that is not hyperbolic was first constructed by Rips in 1982 [53], while a finitely presented subgroup was exhibited by Brady in [15]. It is worth noting that every finite type subgroup of a hyperbolic group of cohomological dimension 2 is hyperbolic [25]. The cohomological dimensions of the groups G and H that are built to prove Theorem B are 5 and 4.

As a corollary of Theorem B, we obtain the following.

Corollary C: *There is a finite type group H that is not hyperbolic, and does not contain any Baumslag-Solitar subgroup $BS(m, n)$.*

It is well-known that any hyperbolic group G is of finite type, and it does not contain any Baumslag-Solitar subgroup $BS(m, n)$. For some classes of groups, this finiteness condition, together with the absence of Baumslag-Solitar subgroups, is actually sufficient to imply hyperbolicity: some examples are the fundamental groups of 3-manifolds, free-by cyclic groups [16], and more generally the ascending HNN extensions of free groups [46]. However, Corollary C shows that this is not true in full generality, answering another well-known open question, raised by Bestvina [8, Question 1.1], Bridson [12, Question 2.22], Drutu and Kapovich [19, Problem 11.129].

Structure of the thesis

This thesis is organized as follows.

In Chapter 1, we present a procedure to build a hyperbolic manifold, starting from a right-angled hyperbolic polytope and a colouring of its facets. Next, we introduce a very symmetric family of polytopes in dimensions 3 to 8, and we use them as building blocks for the previously mentioned procedure. The resulting manifolds M^n are the main characters of this thesis.

The first part of Chapter 2 is dedicated to the exposition of the two main tools used in this thesis: Bestvina-Brady Morse theory, and a combinatorial game by Jankiewicz, Norin and Wise. Following this, we use these tools to build several examples of maps $f : M^n \to S^1$ and study their critical points. In the last part of the chapter we focus on the case of the manifold M^5, for which we build a fibration over the circle S^1, proving Theorem A.

In Chapter 3, after a short introduction to hyperbolic groups, we use the fibering manifold M^5 to build examples of "exotic" hyperbolic groups, proving Theorem B and Corollary C. These results answer some long-standing open questions in geometric group theory.

Finally, in Chapter 4, we discuss some natural and perhaps interesting questions raised by this work.

Chapter 1

Constructing Manifolds

In this chapter we describe a procedure to build a hyperbolic manifold starting from a right-angled polytope and some combinatorial data. Subsequently, we will apply this procedure to a particular sequence of polytopes to build the manifolds which will be the main topic of interest of this thesis; closely following the paper [29]. To help with computations, we have used a program in Sage, whose code can be found in [63].

We will refer to finite volume right-angled polytopes in an ambient space $\mathbb{X}$, that can be either $\mathbb{S}^n$, $\mathbb{R}^n$ or $\mathbb{H}^n$ (in the last case, the polytope can have both real and ideal vertices). Though we are mostly interested in the hyperbolic case, we will state our theory in a more general context, since examples are often easier to visualize in the spherical and Euclidean models. Moreover, the Euclidean case will be relevant to better understand the cusps of the hyperbolic manifolds.

Throughout the course of this thesis, all hyperbolic manifolds are tacitly assumed to be complete and of finite volume, unless otherwise specified.

1.1 From a colouring to a manifold

There is a general procedure to construct an $\mathbb{X}$-manifold, starting from any right-angled $\mathbb{X}$-polytope and a colouring of its facets. This technique was first described by Vesnin [60] in 1987, taking inspiration from Löbell's construction of the first known compact hyperbolic 3-manifold [39] in 1931.

Definition 1. Let c be a natural number. A *c-colouring* of a right-angled polytope $P \subseteq \mathbb{X}$ is the assignment of one colour from a palette $\{1, ..., c\}$ to each facet of P, with the property that adjacent facets have different colours. We assume that each colour is used to paint at least one facet, i.e., that the assignment map $\mathcal{F}(P) \to \{1, ..., c\}$ is surjective.

A right-angled polytope $P \subset \mathbb{X}$ can be interpreted as an orbifold tessellating the space $\mathbb{X}$. In particular, we get $P = \mathbb{X}/_\Gamma$, where Γ is the right-angled Coxeter group generated by the reflections along the facets of P. A presentation for Γ is given by $\langle\ r_F \mid r_F^2, [r_F, r_{F'}]\ \rangle$, where F varies among the facets of P, and F, F' vary among the pairs of adjacent facets.

Given a right-angled $\mathbb{X}$-polytope P with a c-colouring of its facets, we consider the $\mathbb{Z}_2$-vector space $\mathbb{Z}_2^c$, with the canonical basis $e_1, ..., e_c$, and define a homomorphism $\Gamma \to \mathbb{Z}_2^c$ by sending each generator r_F to e_j, where j is the colour of the facet F. One can verify that the kernel Γ' of this map acts freely on $\mathbb{X}$, so we get a manifold $M = \mathbb{X}/_{\Gamma'}$. The resulting manifold M is tessellated in 2^c copies of the polytope P, and of course inherits the elliptic/flat/hyperbolic metric of the model $\mathbb{X}$. The tessellation yields an orbifold cover $M \to P$.

It is interesting to describe this construction from different points of view, that have a more geometric flavour.

The first new description is as follows. We start with the object $M_0 = P$, and then we iteratively double along the facets of each colour. More precisely, we define M_i by taking two copies of M_{i-1} and gluing them along the facets of the colour i (using the identity for the identification). The fact that the polytope has right angles plays a crucial role, since this condition assures that each facet adjacent to the glued ones fuses together with the other copy of itself to a single facet of M_i.

The second description has a more global identity. We start with 2^c copies of P, indexed by vectors $v \in \mathbb{Z}_2^c$, and we explicitly list all the performed gluings. In particular, each facet of colour i of the polytope P_v is glued (with the identity) to the corresponding facet of the polytope P_{v+e_i}.

This construction can be performed in a variety of contexts. Below, we provide some meaningful examples.

Example 2. There is a right-angled spherical n-simplex, that can be coloured with $n+1$ colours, one for each facet. The resulting manifold is S^n, tessellated in 2^{n+1} copies of the simplex. The 2-dimensional example is shown in Figure 1.1.

Example 3. An Euclidean n-cube has right angles, and it can be coloured with n colours, choosing a pair of opposite facets for each colour. The resulting manifold is a flat n-torus T^n, tessellated in 2^n cubes. The 2-dimensional example is shown in Figure 1.2.

Example 4. In the 2-dimensional hyperbolic space, for every $n \geq 5$ there is a compact right-angled hyperbolic n-gon. If n is even, it can be coloured with two colours by

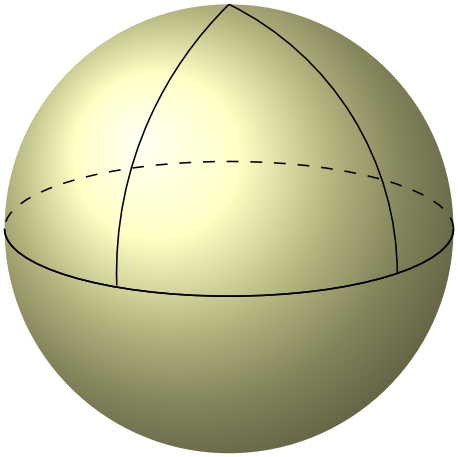

Figure 1.1: A triangle with three right angles in the 2-sphere. By colouring each side with a different colour, we obtain an octahedral tessellation of S^2.

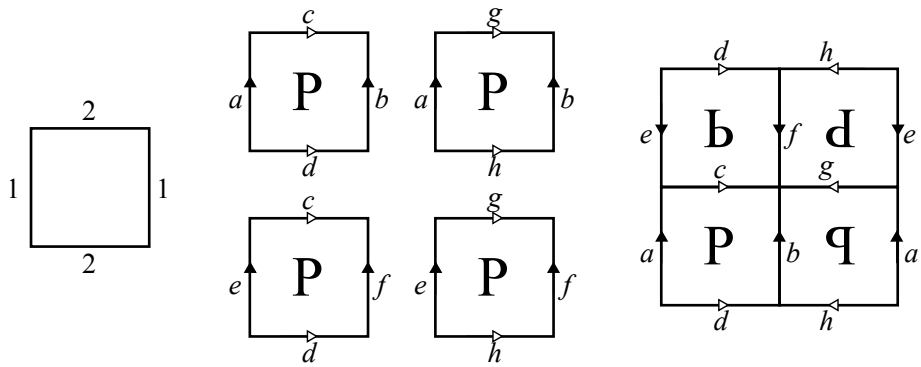

Figure 1.2: On the left, a 2-coloured square. The picture shows the second geometric point of view for the construction: we take $2^2 = 4$ copies of the square, and glue them with the information encoded by the colouring. We obtain a flat torus, as explained in Example 3.

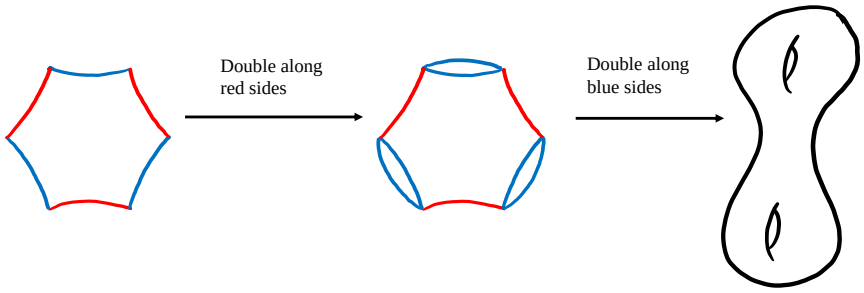

Figure 1.3: On the left, a 2-coloured hyperbolic right-angled hexagon. The picture shows the first geometric point of view for the construction: we iteratively double the picture along each of the colours. We obtain a hyperbolic surface of genus 2, as explained in Example 4.

alternating between the sides. The resulting manifold is a closed surface of genus $\frac{n}{2} - 1$: this can be shown by computing the Euler characteristic. The case of the right-angled hexagon is shown in Figure 1.3.

Example 5. Every ideal hyperbolic polygon is actually right-angled (there are no vertices, and thus there are also no angles). In particular, since the edges are pairwise disjoint, it can be coloured with only one colour. The resulting manifold is simply the double of the polygon, and it is a punctured sphere.

Example 6. The ideal regular octahedron in $\mathbb{H}^3$ is right-angled, and can be coloured with two colours in a checkerboard pattern. The cusped 3-manifold produced by this construction is the complement of the minimally twisted chain link with 6 components. More details can be found in [37].

Example 7. There is a regular right-angled dodecahedron in $\mathbb{H}^3$, which is compact. It is possible to colour it with 4 colours, dividing the 12 faces into triples, as shown in Figure 1.4. The resulting manifold is a closed hyperbolic 3-manifold, tessellated into $2^4 = 16$ copies of such dodecahedron.

Example 8. The ideal 24-cell in $\mathbb{H}^4$ has a unique 3-colouring, up to isomorphism. To describe it, we give a colouring of the vertices of the dual of 24-cell, that is the 24-cell

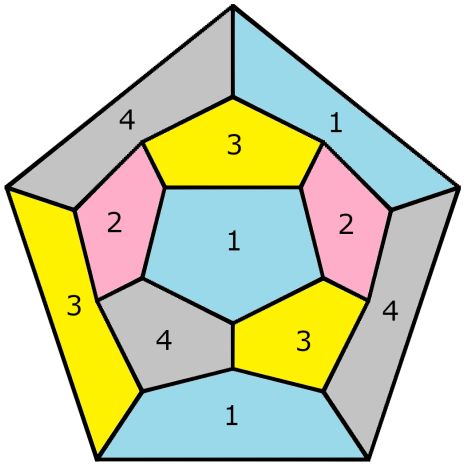

Figure 1.4: A bird's eye view of a 4-colouring of a dodecahedron. The twelfth face is hidden, and it is coloured with the pink (2) colour.

itself. One simple description arises from the quaternion space. The 24 vertices of 24-cell correspond to the quaternions $\pm 1, \pm i, \pm j, \pm k$ and all the 16 choices of signs for $\frac{1}{2}(\pm 1 \pm i \pm j \pm k)$. The edges correspond precisely to the pair of vertices whose scalar product is $\frac{1}{2}$.

We colour them using three colours; the first one involves the 8 vertices $\pm 1, \pm i, \pm j, \pm k$, we use the second to paint the ones of type $\frac{1}{2}(\pm 1 \pm i \pm j \pm k)$ with an even number of minus signs, and the third to paint the ones of type $\frac{1}{2}(\pm 1 \pm i \pm j \pm k)$ with an odd number of minus signs. An alternative way to look at this subdivision is as the orbits of the action of the group $\{\pm 1, \pm i, \pm j, \pm k\}$ over the 24 vertices.

This manifold has been studied in [37], and we refer to this paper for more details.

1.2 Cusps and their sections

If the polytope $P \subset \mathbb{H}^n$ has some ideal vertices, than the manifold resulting from the previous construction will have some cusps. The number of cusps and their shape can be obtained from the initial data by looking at the combinatorial structure of the links of the ideal vertices.

Let $v \in P$ be an ideal vertex. By definition, the link of v in P is the intersection of P with a small horosphere centered at v. Let $C = lk(v)$ be this link; we observe that it is an Euclidean $(n-1)$-polytope (since it is contained in the horosphere) and it is right-angled (since P itself is right-angled). Thus it must be a rectangular cuboid. The cuboid C inherits its own colouring from the colouring of P. Each $(n-2)$-facet

of C corresponds to one $(n-1)$-facet of P (precisely, the one in which it is contained), so we can assign corresponding colours of the facets of P to corresponding facets of C. With this natural choice, the cuboid C is coloured with $c' \leq c$ colours: if we apply the construction to the coloured polytope C, we obtain a flat (closed) $n-1$ manifold N, tessellated in $2^{c'}$ copies of C. If we consider the preimage of C under the cover $M \to P$, we get some copies of N by construction. Since we have in total 2^c copies of C, and each copy of N involves $2^{c'}$ copies of C; the number of copies of N is $2^{c-c'}$.

In summary, the number of cusps that correspond to an ideal vertex v is 2^h, where h is the number of colours that are not assigned to any facets incident to v. The section of those cusps is obtained by restricting the colouring of P to the link C of v, and applying the same construction to it. We next provide some examples.

- If P is a 1-coloured ideal n-gon in $\mathbb{H}^2$, then we saw before that the corresponding manifold is a sphere with n punctures. The link of the ideal vertices is a segment, and it is 1-coloured. As predictable, since every vertex touches all the colours, there is just $2^0 = 1$ cusp over each vertex, and the section is a circle obtained by gluing two segments by their endpoints.

- If P is an ideal n-gon in $\mathbb{H}^2$ with all sides coloured with one colour except for one side, we can check that the resulting manifold is a sphere with $2n-2$ punctures. There are vertices of two types: vertices adjacent to sides of the same colour, and the two vertices adjacent to the special side. In the first case, the link is a segment with the endpoints of the same colour. As before, the section of a cusp is a circle tessellated is two segments, but this time there is a colour that is not used and so we get $2^1 = 2$ cusps corresponding to such vertices. In the latter case, the link is still a segment, but its endpoints are coloured with only one colour. This way, we get only one cusp with circular section, but it is in some sense "larger" then before, since it is tessellated in four segments.

- If P is an ideal n-gon in $\mathbb{H}^2$ and we colour its sides with n different colours, then all ideal vertices will have sections that are circles tessellated in four segments, and each one of them will have 2^{n-2} cusps corresponding to it. The resulting manifold is a surface with $n \cdot 2^{n-2}$ punctures. By computing its Euler characteristic, it is possible to see that it has genus $1 + (n-4) \cdot 2^{n-3}$.

- If P is the ideal regular octahedron in $\mathbb{H}^3$ and we colour it with two colours in a checkerboard pattern as in Example 6, the link of each of the 6 ideal vertices is a square. For each of these vertices we have that $h = 0$, and the square is coloured with two colours, giving raise to a torus. Then we have 6 cusps in total,

which correspond to what was previously stated: the resulting manifold is the complement of the minimally twisted chain link with 6 components.

- If P is the ideal 24-cell in $\mathbb{H}^4$, with the 3-colouring described in Example 8, there are 24 ideal vertices whose link is a 3-cube. Since every cube needs to be coloured with at least 3 colours, and we are using 3 colours in total, each link is a 3-coloured 3-cube. Hence, $h = 0$, and so the resulting manifold M has 24 toric cusps in total.

Cuboid gluings in cusp sections

As we have already discussed, the link of an ideal vertex of a hyperbolic polytope lives in a horosphere, therefore it has a natural Euclidean metric. Since we are considering only right-angled polytopes, the only possibility for it is to be a rectangular cuboid. In this section, we study what can happen to such cuboids when we apply the colouring construction.

We start by considering a general Euclidean n-dimensional cuboid

$$C = [0, \ell_1] \times ... \times [0, \ell_n]$$

The cuboid C has $2n$ facets, and only the opposite facets do not touch. Therefore, the smallest colouring uses n colours, one for each opposite pair. Any c-colouring of C has $n \leq c \leq 2n$, and it is determined by the property that $2n - c$ opposite pairs share the same colour, while the remaining $2(c - n)$ pairs have different colours. If we consider C to be a cube (which is the case, if we limit ourselves to the combinatorial point of view), the number of colours c completely determines the colouring, up to isometries of C. Let N be the flat n-manifold resulting by applying the usual construction to the coloured cuboid C.

Proposition 9. *The resulting flat manifold N is an n-torus, and it is isometric to the product of n circles of length $a_1\ell_1, ..., a_n\ell_n$ where $a_i = 2$ if the i-th pair of opposite faces share the same colour, and $a_i = 4$ otherwise.*

Proof. We use the algebraic definition of the construction. Therefore let us consider Γ to be the reflection group of C and $\Gamma' \triangleleft \Gamma$ be the kernel of the map $\Gamma \to \mathbb{Z}_2^c$ induced by the colouring. By definition, we have that $M = \mathbb{R}^n/\Gamma'$.

We now consider $r_{i,1}$ and $r_{i,2}$ to be the reflections along the opposite facets of C that are orthogonal to the i-th axis, for $i = 1, \ldots, n$. The composition $r_{i,1}r_{i,2}$ is a translation along the axis of distance $2\ell_i$. If the facets share the same colour, we have $r_{i,1}r_{i,2} \in \Gamma'$. Otherwise, we have $r_{i,1}r_{i,2}r_{i,1}r_{i,2} \in \Gamma'$. This shows that

$$a_1\ell_1\mathbb{Z} \times \cdots \times a_n\ell_n\mathbb{Z} < \Gamma'$$

where a_i is equals to either 2 or 4, depending on whether the i-th pair of opposite facets shares the same colour.

To show that they are actually equal, we show that these two subgroups have the same index in Γ. If we use c colours, we have noted before that $2n - c$ opposite pairs share the same colour, while the remaining $2(c - n)$ pairs have different colours. We deduce that the two indices of those groups in Γ are

$$2^{2n-c} \cdot 4^{c-n} = 2^c.$$

Therefore $\Gamma' = a_1\ell_1\mathbb{Z} \times \cdots \times a_n\ell_n\mathbb{Z}$ and M is as stated. □

Summing up our discussion on the cusps of the hyperbolic manifolds arising from the colouring construction, we get the following:

Proposition 10. *Let $P \subset \mathbb{H}^n$ a right-angled polytope with some ideal vertices, let us consider a c-colouring of P, and let M be the hyperbolic n-manifold resulting from the construction. Then:*

(i) All the cusps of M are toric, i.e., they are diffeomorphic to a flat $(n-1)$-torus;

(ii) For every ideal vertex v, the number of cusps above v is $2^{c-c'}$, where c' is the number of colours of facets incident to v.

1.3 Right-angled hyperbolic polytopes

After having described the procedure, we now turn our attention to its main ingredient: right-angled polytopes. While in Euclidean geometry only cuboids have right angles, hyperbolic geometry has a richer variety, at least when the dimension is low enough.

In $\mathbb{H}^2$, there are plenty of right-angled n-gons for each $n > 4$, and we can even choose some of the vertices to be ideal. In dimensions 3 and 4 we have plenty of interesting examples, both compact and non-compact, such as the previously mentioned regular dodecahedron and the ideal regular octahedron in $\mathbb{H}^3$, or (the compact) regular 120-cell and the ideal regular 24-cell in $\mathbb{H}^4$.

Compact right-angled hyperbolic polytopes cannot exist when the dimension is higher then 4: this follows from Nikulin inequality [47] for the average number of h-dimensional faces of a k-dimensional face of a simple polytope (see [48] for more details). As a consequence, it is impossible to build closed hyperbolic manifolds in dimension higher than 4 using the techniques described in this chapter.

It has been also proven by Dufour that right-angled hyperbolic polytopes cannot exist when the dimension is higher than 12, (see [20]).

Finally, examples are only known up to dimension 8, some of which will be present in the next section.

1.4 The polytopes P^n

We now present the sequence of polytopes that will be use as the main building blocks in this thesis. It is a sequence of right-angled hyperbolic polytopes P^2, P^3, P^4, P^5, P^6, P^7, P^8 with both ideal and real vertices, which have very nice symmetries. These polytopes were first introduced in a paper of Agol, Long and Reid [2]. A complete description of the combinatorial and geometric properties of these polytopes can be found in [48] and [21], but we briefly summarize here the main properties and how they are constructed.

For each $n = 2, ..., 8$ the polytope $P^n \subset \mathbb{H}^n$ is an n-dimensional finite-volume hyperbolic right-angled polytope with both ideal and real vertices. The real vertices all have a $(n-1)$-simplex as a link, while all the links of the ideal vertices are a $(n-1)$-cube. All the facets of the polytope P^n are isometric to P_{n-1}. Moreover, the isometry group of each P^n acts transitively on the facets. A summary of the main combinatorial features of such polytopes is illustrated in Table 1.1.

The polytope P^2 is a triangle with two ideal vertices and one real vertex that has a right angle. We can describe P^2 as the result of a construction procedure that will be useful to understand the higher dimensional polytopes. We start by taking two copies of a hyperbolic triangle Δ^2 with one ideal vertex and the remaining two angles of $\frac{\pi}{2}$ and $\frac{\pi}{4}$; we then glue those two triangles along the side with the two real vertices. Note that both angles double; so we get a right angle in correspondence of the $\frac{\pi}{4}$ of Δ^2. The two right angles fuse together into an angle of π, so the two sides glue nicely into a single side. A picture of this gluing can be found in Figure 1.5.

To build the polytope P^n we start from a hyperbolic Coxeter n-simplex Δ^n with one facet F^* that has the following properties:

1. The angle between F^* and all the other facets is either $\frac{\pi}{2}$ or $\frac{\pi}{4}$.
2. The vertex v^* opposite to F^* is real.

Such a simplex exists up to dimension 8. Since Δ^n is a hyperbolic Coxeter polytope, it tessellates $\mathbb{H}^n$. Inside this tessellation we can consider one vertex corresponding to v^*, and define P^n to be the star of this vertex (i.e., the union of all the simplices that contain this vertex). Analogously to what we have seen before, the angles of $\frac{\pi}{4}$ will fuse in pairs to form right angles, and the right angles will make an angle of π that fuses the facets together, thus eliminating the angle. A picture of this process for P^3 is shown in Figure 1.6.

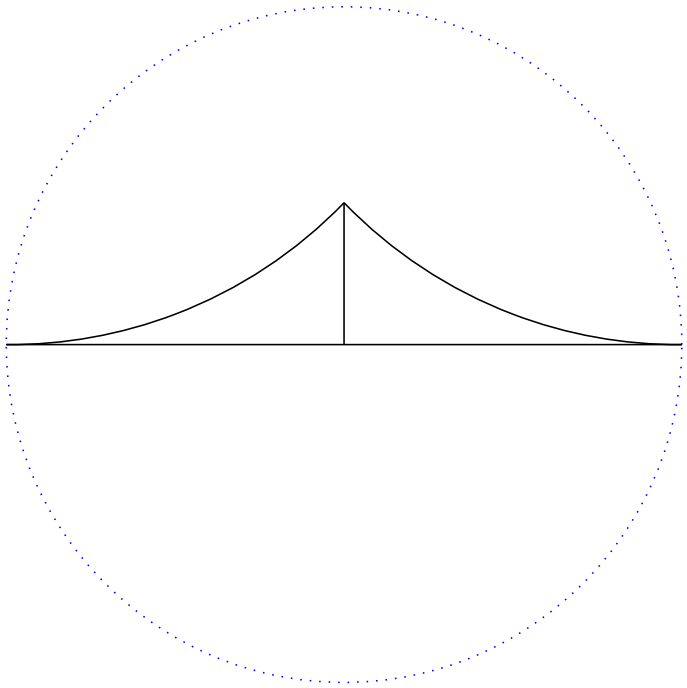

Figure 1.5: The polygon P^2 inside the hyperbolic plane $\mathbb{H}^2$. It is the union of two hyperbolic triangles with one ideal vertex and angles $(0, \frac{\pi}{4}, \frac{\pi}{2})$. Note that the two horizontal sides near the right angles fuse together into a single side.

	Facets	Ideal	Finite	Isom(P^n)	#Isom(P^n)	Dual
P^3	6	3	2	$A_1 \times A_2$	12	Triangular prism
P^4	10	5	5	A_4	120	Gosset 0_{21}
P^5	16	10	16	D_5	1920	Gosset 1_{21}
P^6	27	27	72	E_6	51840	Gosset 2_{21}
P^7	56	126	576	E_7	2903040	Gosset 3_{21}
P^8	240	2160	17280	E_8	696729600	Gosset 4_{21}

Table 1.1: The number of facets, ideal vertices, and finite vertices of P^n, the isometry group Isom(P^n) expressed as a Weyl group and its order $|\text{Isom}(P^n)|$, and the dual Euclidean polytope.

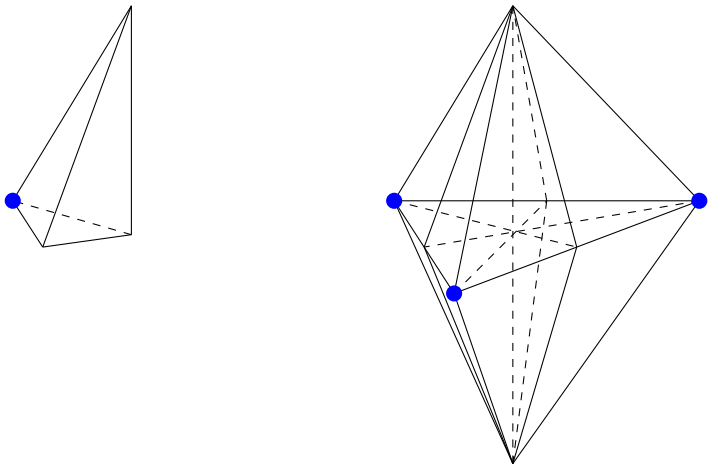

Figure 1.6: On the left, the simplex Δ^3. The bottom face is F^*, and has angles of $\frac{\pi}{2}, \frac{\pi}{2}, \frac{\pi}{4}$ with the other faces. The other 3 faces make angles of $\frac{\pi}{2}, \frac{\pi}{4}, \frac{\pi}{6}$ with each other. On the right, the subdivision of P^3 into 12 simplices given by its construction process. The ideal vertices are marked with a blue dot.

The dual Gosset polytopes

For the constructions used in this thesis, we are especially interested in the combinatorial dual of the polytopes we intend to use. The dual of the polytopes P^n is a remarkable sequence of polytopes that was discovered and studied by Gosset [26] in 1900. Every Gosset polytope is a Euclidean polytope with regular facets, whose isometry group (which is the same as $\mathrm{Isom}(P^n)$) acts transitively on the vertices. Its regular facets are of two types: facets that are dual to the real vertices of P^n are simplices, and facets that are dual to the ideal vertices of P^n are hyperoctahedra. This is of course expected, as they are the dual of the links of such vertices in P^n.

A colouring on P^n corresponds to a colouring of the vertices of the dual Gosset polytope such that vertices that are connected by an edge must have different colours. To do that, we will consider the 1-skeleton of the Gosset polytopes, and try to find a colouring that respects as much as possible the following two principles:

- It has a small number of colours;

- It has a high degree of symmetry, which means that a large number of isometries preserve the colouring.

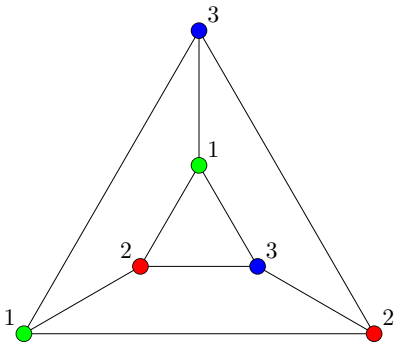

Figure 1.7: The chosen colouring on the dual of P^3. Each of the three lateral squares corresponds to an ideal vertex.

1.5 The manifold M^3

The polytope P^3 is a right-angled double pyramid with triangular base. It has three ideal vertices (corresponding to the base triangle), and two real vertices. The dual polytope is a triangular prism: its 1-skeleton can be coloured with three colours as shown in Figure 1.7. This colouring is unique up to isomorphism, and uses the minimal number of colours. We assign this colouring to P^3, and apply the previous construction to it: this produces a hyperbolic 3-manifold M^3, tessellated in $2^3 = 8$ copies of P^3.

The polytope P^3 has three ideal vertices, each of them having a square C as link, since they correspond to the square faces in the dual triangular prism. As we can see in Figure 1.7, every square C is 3-coloured. By Proposition 10, we deduce that every ideal vertex corresponds to a unique cusp, since $2^{3-3} = 1$. The manifold M^3 has therefore 3 toric cusps.
Using Sage, and a formula from [18], we were able to compute the Betti numbers of M^3:

$$b_0(M^3) = 1, \qquad b_1(M^3) = 3, \qquad b_2(M^3) = 2.$$

Finally, we are able to describe more explicitly the manifold M^3:

Theorem 11. *The manifold M^3 is the complement of the Borromean rings in S^3.*

Proof. Let $C = [0,1]^3$ be a cube. Remove from C the three edges of equation

$$x = 1,\ y = 0; \qquad y = 1,\ z = 0; \qquad z = 1,\ x = 0.$$

A picture of the resulting cube can be found in Figure 1.8. If we think of those edges as ideal vertices, C could be seen as a polyhedron which is combinatorially isomorphic

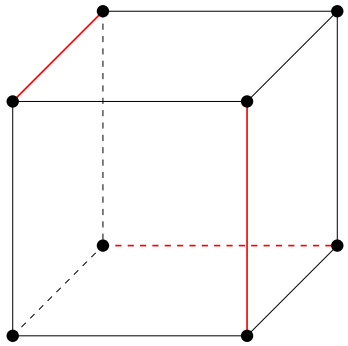

Figure 1.8: A representation of P^3 as a cube with 3 edges removed.

to P^3; the two real vertices are $(0,0,0)$ and $(1,1,1)$, and the 6 faces of the cube become triangular after having collapsed the three edges to (ideal) vertices.

We now describe M^3 by using C instead of P^3. We colour C with 3 colours exactly as we have done for P^3. After having performed the construction, we obtain a 3-torus tessellated in 8 copies of a cube, with three lines removed (corresponding to the edges removed in C), parallel to the vectors $(1,0,0)$, $(0,1,0)$ and $(0,0,1)$. The three lines removed are exactly the cores of the solid tori glued in the representation of the 3-torus as the $(0,0,0)$-Dehn filling of the complement of the Borromean rings in S^3. Hence, the Theorem follows. □

1.6 The manifold M^4

The polytope P^4 has 10 facets (each of which is isometric to P^3), 5 real vertices and 5 ideal vertices. A detailed description can be found in [48] and [51]. As stated before, the dual of P^4 is the Gosset polytope 0_{21}, which is the 4-dimensional rectified simplex. To visualize 0_{21}, we can see it as the convex hull of the midpoints of the 10 edges of a 4-dimensional simplex. More explicitly, the 10 vertices of 0_{21} can be seen in $\mathbb{R}^5$ as the points which have two coordinates equal 1, and all the other coordinates equal to 0. Two vertices are connected by an edge if they differ by exactly two coordinates. Furthermore, there are 10 facets; 5 of them are regular tetrahedra, and the other 5 facets are regular octahedra. The tetrahedral facets are created by the rectification process, and correspond to the real vertices of P^4; while the octahedral facets are the remaining part of the original facets after the rectification cut, and correspond to the ideal vertices of P^4.

A projection of the 1-skeleton of 0_{21} is shown in Figure 1.9. In Figure 1.10 we show

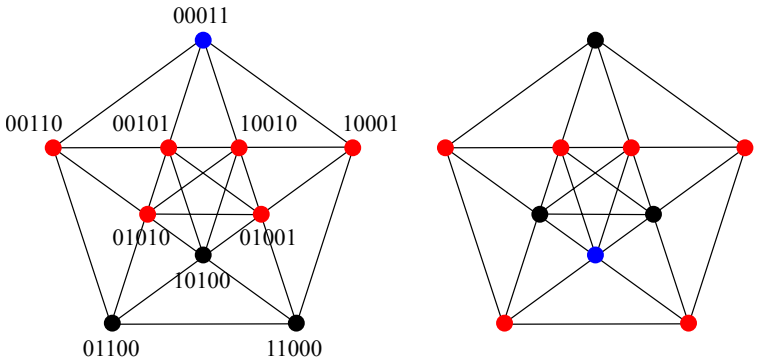

Figure 1.9: A projection of the 1-skeleton of the rectified simplex 0_{21} on the plane, we also show the string of 0 and 1 representing the coordinates of those points in $\mathbb{R}^5$. Some caution is needed here and in the subsequent figures, since some edges are superposed, so two vertices that are connected by an edge on the plane projection may not be so in 0_{21}. To clarify this ambiguity, we have chosen a blue vertex and painted in red the 6 vertices adjacent to it, in two cases (all the other cases are obtained by rotation). The blue and black vertices are non-incident. In general, two vertices that belong to a line that crosses the center of the figure are non -incident. There are 5 such lines, and they partition the 10 vertices into 5 pairs.

a 5-colouring for 0_{21}, and hence P^4. By assigning this colouring to P^4, we obtain a hyperbolic manifold P^4 tessellated in $2^5 = 32$ copies of P^4.

We now look into the ideal vertices of P^4, i.e., the octahedral facets of 0_{21}. As we have seen, there are 5 such facets in 0_{21}, and each of them is contained in one of the five coordinate hyperplane $x_i = 0$. In Figure 1.11 we highlight the facet corresponding to $x_1 = 0$, and see that it is 5-coloured; the same holds for the other four octahedra. By duality, we have that the link of each ideal vertex of P^4 is a 5-coloured cube. Thus, by Proposition 10, we deduce that every ideal vertex corresponds to a unique toric cusp, since $2^{5-5} = 1$. The manifold M^4 has therefore 5 cusps.
Using Sage, and a formula from [18], we were able to compute the Betti numbers of M^4:

$$b_0(M^4) = 1, \qquad b_1(M^4) = 5, \qquad b_2(M^3) = 10, \qquad b_3(M^4) = 4.$$

We get $\chi(M^4) = 2$.

1.7 The manifold M^5

The polytope P^5 has 16 facets (each of which is isometric to P^4), 16 real vertices and 10 ideal vertices. Each facet is opposed to a real vertex. A more detailed description

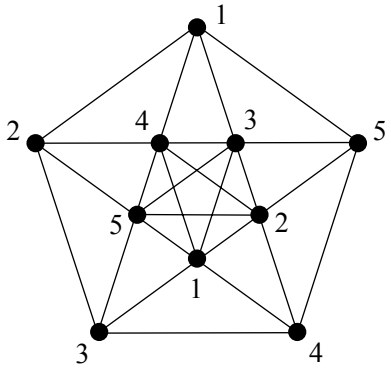

Figure 1.10: A 5-colouring of the 1-skeleton of the Gosset polytope 0_{21}, corresponding to our choice of colouring for P^4.

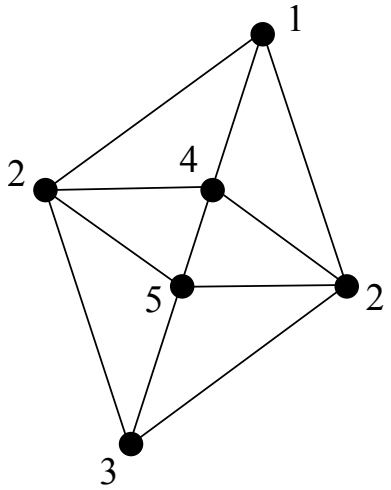

Figure 1.11: The octahedral facet of P^4 corresponding to the hyperplane $x_1 = 0$, and the colouring it inherits. This is a subgraph of Figure 1.10.

can be found in [48] and [52].

To describe P^5 we can use the Klein model for $\mathbb{H}^5$, seen as the unit ball embedded in $\mathbb{R}^5$. In this way, we can see it both as an hyperbolic and an Euclidean polytope, depending on the situation. The polytope P^5 is the intersection of the 16 half-spaces of equation

$$\pm x_1 \pm x_2 \pm x_3 \pm x_4 \pm x_5 \leq 1$$

having an even number of minus signs. The 10 ideal vertices correspond to the points

$$(\pm 1, 0, 0, 0, 0), \quad (0, \pm 1, 0, 0, 0), \quad (0, 0, \pm 1, 0, 0), \quad (0, 0, 0, \pm 1, 0), \quad (0, 0, 0, 0, \pm 1).$$

The 16 real vertices are the points

$$\frac{1}{3}(\pm 1, \pm 1, \pm 1, \pm 1, \pm 1).$$

having an odd number of minus signs. Each of this vertices is opposed to a facet of P^5 (precisely, the one with the equation that has the opposite choices of signs).

As stated before, the dual of P^5 is the Gosset polytope 1_{21}. We can represent 1_{21} in $\mathbb{R}^5$ by describing it as the convex hull of the vertices $(\pm 1, \pm 1, \pm 1, \pm 1, \pm 1)$ with an odd number of minus signs. Two vertices are connected by an edge if they differ by exactly two coordinates. Furthermore, there are 26 facets; 16 of them are regular 4-simplices (corresponding to the real vertices of P^5), and the other 10 are regular 4-octahedra (corresponding to the ideal vertices).

In Figure 1.12 we have shown a representation of the 1-skeleton of 1_{21}. It is based on the fact that the first 4 coordinates determine the last one (since there is an odd number of minus signs); so we can represent it as a hypercube. We have said before that the edges correspond to a difference in two coordinates; if one of those coordinates is the last one, they correspond to edges of the hypercube, otherwise they correspond to a diagonal of a 2-face. Another representation of the 1-skeleton of 1_{21}, which is a projection similar to the one drawn in the case of P^4, is shown in Figure 1.13. The polytope 1_{21} has 26 facets: 16 of them are regular 4-simplices and correspond to the real vertices of P^5, while the other 10 are regular 4-octahedra dual to ideal vertices of P^5. The 10 octahedra will play a slightly different role than before, since they will be distinguished by the colouring into two types.

The hypercube representation shows that there are 8 pairs of vertices (the ones that are opposite to each other) that are not adjacent to each other; we can use 8 colours to colour them as shown in Figure 1.14.

Performing the usual construction with this colouring gives rise to a hyperbolic 5-manifold tessellated in $2^8 = 256$ copies of P^5.

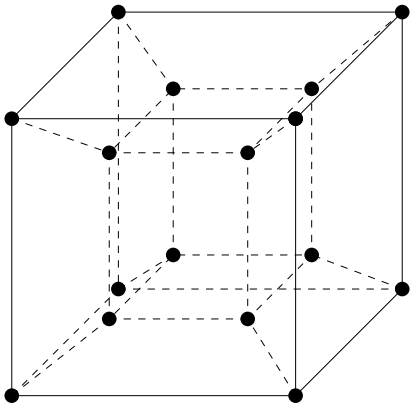

Figure 1.12: A representation of the 1-skeleton of a hypercube. To obtain the 1-skeleton of 1_{21} it would be necessary to add all the diagonals of all the square faces, but we avoid to draw them for better readability. Instead, one should consider two vertices to be adjacent if and only if they are connected by a path of length ≤ 2.

We now look at the ideal vertices of P^5, which correspond to the octahedral facets of 1_{21}. Each of those facets is contained in one of the 10 hyperplanes of equation $x_i = \pm 1$. Since our colouring is not symmetric in the five coordinates, the two facets on the hyperplanes $x_5 = \pm 1$ will inherit a colouring that is different from the other 8 facets. The two cases are shown in Figure 1.15 and Figure 1.16.

The picture on the left of Figure 1.15 shows the 8 ideal vertices whose link gets a colouring with all 8 colours. In this case by Proposition 10, over the vertex there is only one (toric) cusp, since $2^{8-8} = 1$. We will call those the large cusps. On the right of Figure 1.15, we have a representation of one of the two other links: since they inherit a colouring with only four colours, by Proposition 10 we get $2^{8-4} = 16$ cusps over each vertex. The manifold M^5 has therefore $8 \cdot 1 + 2 \cdot 16 = 40$ cusps.

With the usual Sage program, we were able to compute the Betti numbers of M^5:

$$b_0 = 1, \qquad b_1 = 24, \qquad b_2 = 120, \qquad b_3 = 136, \qquad b_4 = 39.$$

We get $\chi(M^5) = 0$, as expected.

1.8 The manifold M^6

The polytope P^6 has 27 facets, each one isometric to P^5. It has 72 real vertices and 27 ideal vertices, each of which is opposed to a facet. As always, we refer the reader to [21] and [48] for more details.

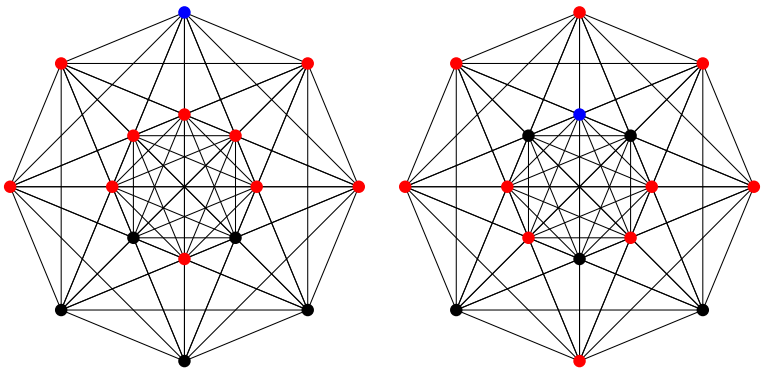

Figure 1.13: A projection of the 1-skeleton of the Gosset polytope 1_{21} on the plane. Some caution is needed here and in the subsequent figures, since some edges are superposed, so two vertices that are connected by an edge on the plane projection may not be so in 1_{21}. To clarify this ambiguity, we have chosen a blue vertex and painted in red the 6 vertices adjacent to it, in two cases (all the other cases are obtained by rotation). The blue and black vertices are non-incident.

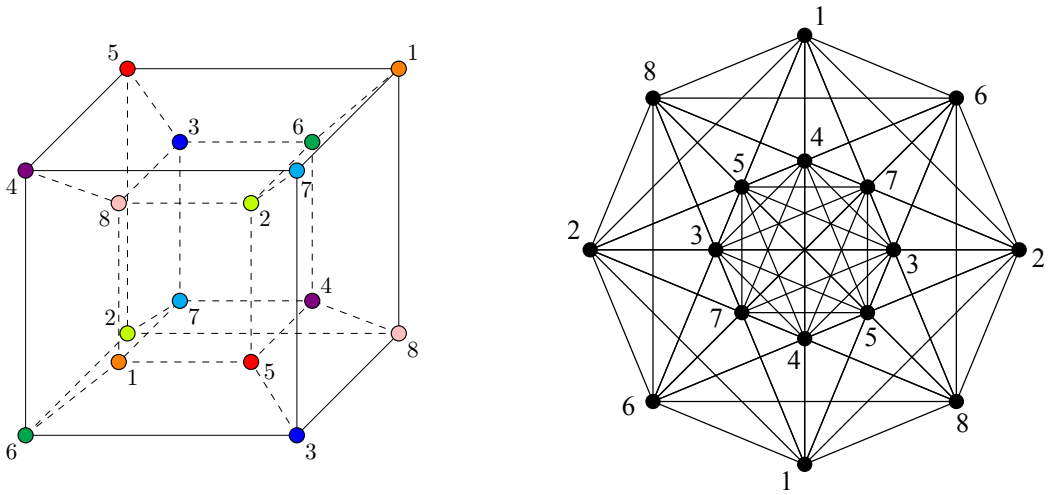

Figure 1.14: A 8-colouring of the 1-skeleton of the Gosset polytope 1_{21}, corresponding to our choice of colouring for P^5. We show the colouring in both models we presented in the previous figures. Pairs of colours with labels $(t, t+4)$ have a similar shade, foreshadowing the pairing that will be implemented in Section 2.8.

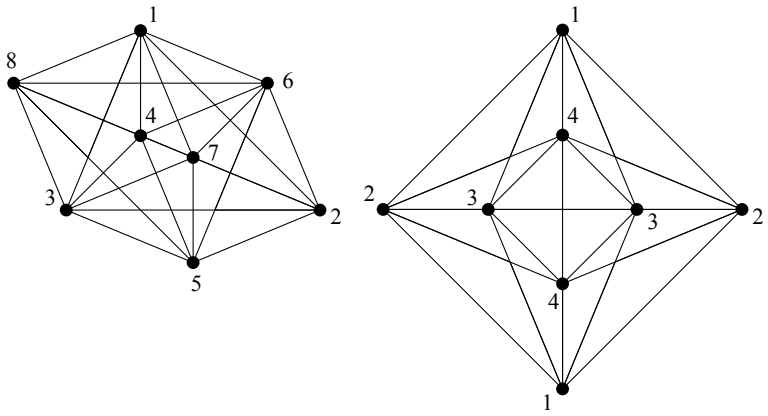

Figure 1.15: The 4-octahedral facets of 1_{21} may inherit one of two different kinds of colouring. Eight of them inherit a colouring similar to the one of the picture on the left, while the remaining two inherit a colouring such as the one on the right. Since these are subgraphs of Figure 1.13, some edges are still superposed.

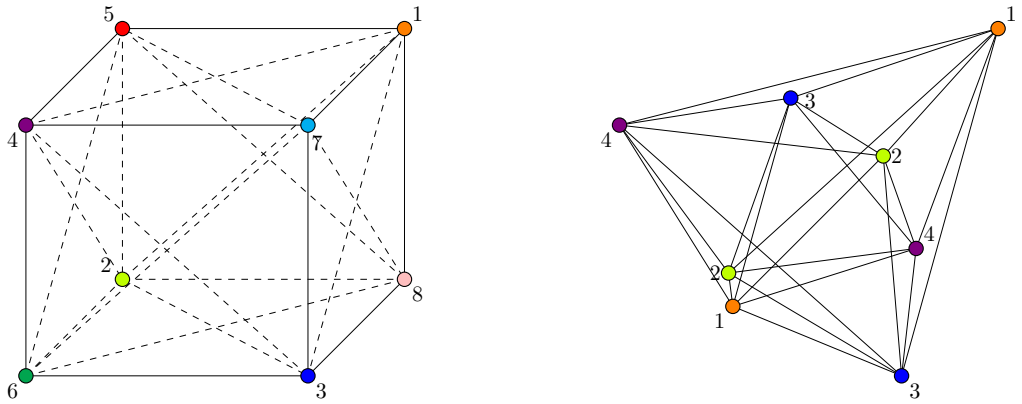

Figure 1.16: The 4-octahedral facets of 1_{21} in the hypercube picture of 1_{21}. We show all the edges, even the diagonal ones hidden in Figure 1.12. Eight of them inherit a colouring similar to the one of the picture on the left, and correspond to the vertices of 8 facets of the hypercube in the picture. The remaining two inherit a colouring such as the one on the right.

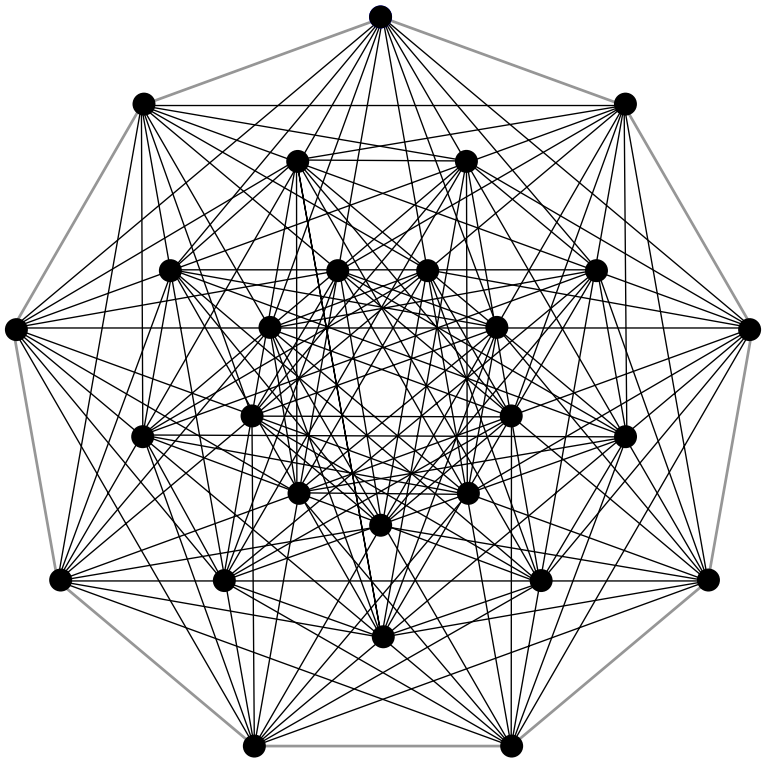

Figure 1.17: A projection of the 1-skeleton of 2_{21} on the plane. As always, some caution is needed, since some edges are superposed, and therefore two vertices that are connected by an edge in the planar projection may not be so in 2_{21}.

The dual of P^6 is the Gosset polytope 2_{21}, which has of course 27 vertices and $99 = 27 + 72$ facets. We can represent the polytope 2_{21} in $\mathbb{R}^7$, contained in the affine hyperspace of equation $x_1 + ... + x_6 - 3x_7 = -1$, by choosing as vertices all the points that can be obtained by permuting the first six coordinates of the following three points:

$$(-1, 0, 0, 0, 0, 0, 0), \qquad (1, 1, 0, 0, 0, 0, 1), \qquad (0, 1, 1, 1, 1, 1, 2)$$

Two vertices are connected by an edge if their Lorentzian product is 0. There are 99 facets in total, 72 of those are regular 5-simplices (corresponding to the real vertices), and the remaining 27 are the 5-octahedra dual to the ideal vertices. Similarly to what we have done in the previous case, we draw a planar projection of the 1-skeleton of 2_{21} in Figure 1.17.

We now describe a colouring for P^6. We divide all the vertices of P^6 into the following triplets of mutually disjoint vertices:

(-1,0,0,0,0,0,0), (1,1,0,0,0,0,1), (1,0,1,1,1,1,2);
(0,-1,0,0,0,0,0), (0,1,1,0,0,0,1), (1,1,0,1,1,1,2);
(0,0,-1,0,0,0,0), (0,0,1,1,0,0,1), (1,1,1,0,1,1,2);
(0,0,0,-1,0,0,0), (0,0,0,1,1,0,1), (1,1,1,1,0,1,2);
(0,0,0,0,-1,0,0), (0,0,0,0,1,1,1), (1,1,1,1,1,0,2);
(0,0,0,0,0,-1,0), (1,0,0,0,0,1,1), (0,1,1,1,1,1,2);
(1,0,1,0,0,0,1), (0,1,0,0,1,0,1), (0,0,0,1,0,1,1);
(0,1,0,1,0,0,1), (0,0,1,0,0,1,1), (1,0,0,0,1,0,1);
(0,0,1,0,1,0,1), (1,0,0,1,0,0,1), (0,1,0,0,0,1,1).

The colouring produces a hyperbolic 6-manifold M^6, that is tessellated into $2^9 = 512$ copies of the polytope P^6.

The polytope P^6 has 27 ideal vertices. Using our program in Sage [63], it is possible to verify that the link of each of these 27 ideal vertices is a 9-coloured 5-cube C. In fact, each ideal vertex v is opposed to a facet F of P^6, and v is incident precisely to the 10 facets that are not adjacent to F. Therefore, by Proposition 10, the preimage of C consists of a single toric cusp section (since $2^{9-9} = 1$). In particular, we deduce that the hyperbolic manifold M^6 has 27 cusps, one above each vertex of P^6.

The Betti numbers of M^6, calculated by our program, are:

$$b_0 = 1, \qquad b_1 = 18, \qquad b_2 = 183, \qquad b_3 = 411, \qquad b_4 = 207, \qquad b_5 = 26.$$

We get $\chi(M^6) = -64$.

1.9 The manifold M^7

The hyperbolic polytope P^7 has 56 facets, each isometric to P^6. It has 576 real vertices, and 126 ideal vertices.

The dual Gosset polytope 3_{21} has 56 vertices. Our choice of colouring will be based on the fact that P^7 is a facet of P^8, and therefore a colouring of P^8 induces a colouring of P^7. This is simply done by choosing a facet F of P^8, that it is isometric to P^7, and noticing that the facet of F are characterized as the intersection of F with one of the other facets of P^8 that are adjacent to F. We use such correspondence to assign colours to F, hence to P^7. We notice that we use at least one colour less then in the original colouring, since the colour of F will not be present in its adjacent facets.

In particular, starting from a specific 15-colouring of P^8, that will be described in Section 1.10, we will notice that it induces a 14-colouring on P^7. We equip P^7 with this 14-colouring. The usual construction produces a hyperbolic 7-manifold M^7, tessellated into $2^{14} = 16384$ copies of P^7.

The polytope P^7 has 126 ideal vertices. To compute the number of cusps of M^7 we used Sage to identify how many colours appear in the links of the ideal vertices. We discovered that 14 of these vertices are incident to 6 distinctly-coloured facets (so they generate $2^{14-6} = 2^8$ cusps each), while the remaining 112 are incident to 12 (so they correspond to $2^{14-12} = 4$ cusps. This fact is similar to what happens for P^5, in particular 6 and 12 are again the minimum and maximum number of colours in a colouring of a 6-cube. From Proposition 10 we deduce that M^7 has $14 \cdot 2^8 + 112 \cdot 2^2 = 4032$ cusps.

We used Sage to compute the Betti numbers of M^7:

$$b_0 = 1,\ b_1 = 182,\ b_2 = 6321,\ b_3 = 41300,\ b_4 = 55139,\ b_5 = 24010,\ b_6 = 4031.$$

We get $\chi(M^7) = 0$, as expected.

1.10 The manifold M^8

The hyperbolic polytope P^8 has 240 facets (each of which is isometric to P^6), 17280 real vertices, and 2160 ideal vertices. The dual polytope is the Gosset polytope 4_{21}, which has 240 vertices. Despite its complicated combinatorics, it admits a very symmetric description by using octonions, very similar to the one done with the 24-cell in Example 8.

Octonions

Octonions are a generalization of quaternions to dimension 8. Although they share with quaternions many algebraic and combinatorial properties, one should be careful when operating with them, since the product of octonions is not associative. We will briefly introduce the main features, and we recommend [5] for a more extensive introduction.

We define the octonions $\mathbb{O}$ as the $\mathbb{R}$-vector space of basis $1, e_1, ..., e_7$. We equip it with a multiplication, by imposing that $e_i^2 = -1$ and that $e_i \cdot e_{i+1} = e_{i+3}$ for each index i (indices are intended modulo 7). From the previous data it is possible to deduce the whole multiplication table for $e_i \cdot e_j$, but there is a useful visual representation: the product of two distinct elements e_i and e_j is described by the Fano plane shown in Figure 1.18.

In particular, for every $i \neq j$ the elements e_i and e_j share one oriented line in the diagram; if e_k is the third element of that line, we have that $e_i \cdot e_j = \pm e_k$, where the sign depends on whether the cyclic orientation i, j, k is the same depicted in the oriented line. For example, $e_1 e_2 = e_4$ and $e_3 e_1 = e_7$.

As it happens with quaternions, the product is not commutative. However, in this case, more attention is required.

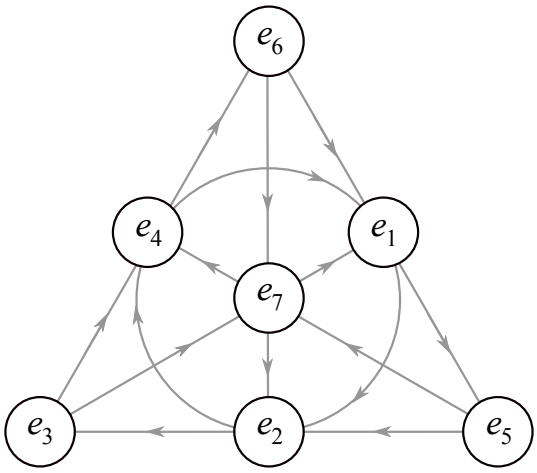

Figure 1.18: The Fano plane, which is the projective plane over $\mathbb{Z}_2$. It contains 7 points and 7 oriented lines (the circle should be interpreted as a line, and all lines should be interpreted as cyclic).

Remark 12. The product in $\mathbb{O}$ is not associative, for example

$$(e_1e_2)e_3 = e_4e_3 = -e_6, \qquad e_1(e_2e_3) = e_1e_5 = e_6.$$

It is in general true that $(e_ie_j)e_k = \pm e_i(e_je_k)$, where the sign is + if and only if e_i, e_j and e_k belong to the same line of the Fano diagram.

The colouring

The Gosset polytope 4_{21} can be nicely represented in $\mathbb{O}$: the vertices are the 240 non-trivial elements of smallest norm in the E_8 lattice (up to rescaling). In particular, the vertices are the octonions

$$\pm 1,\ \pm e_1,\ \pm e_2,\ \pm e_3,\ \pm e_4,\ \pm e_5,\ \pm e_6,\ \pm e_7,$$
$$\tfrac{1}{2}(\pm 1 \pm e_n \pm e_{n+1} \pm e_{n+3}), \qquad \tfrac{1}{2}(\pm e_{n+2} \pm e_{n+4} \pm e_{n+5} \pm e_{n+6})$$

where the index n runs modulo 7. We get indeed $2 \cdot 8 + 16 \cdot 7 + 16 \cdot 7 = 240$ vertices in total. Two such vertices are connected by an edge if and only if their scalar product (as elements of the Euclidean space $\mathbb{R}^8$ is $\frac{1}{2}$). Each vertex is connected to 56 other vertices, this is coherent with the fact that the link is (the dual of) P^7, which has 56 facets.

We subdivide the 240 vertices into 15 groups of 16 vertices each, and use this subdivision as a colouring. The groups are:

1. $C_0 = \{\pm 1, \pm e_1, \pm e_2, \pm e_3, \pm e_4, \pm e_5, \pm e_6, \pm e_7\}$;

2. For each of the 7 possible fixed values of n, we take the set C_n^+ the elements of type $\frac{1}{2}(\pm 1 \pm e_n \pm e_{n+1} \pm e_{n+3})$ and $\frac{1}{2}(\pm e_{n+2} \pm e_{n+4} \pm e_{n+5} \pm e_{n+6})$ that have an even number of minus signs;

3. For each of the 7 possible fixed values of n, we take the set C_n^- the elements of type $\frac{1}{2}(\pm 1 \pm e_n \pm e_{n+1} \pm e_{n+3})$ and $\frac{1}{2}(\pm e_{n+2} \pm e_{n+4} \pm e_{n+5} \pm e_{n+6})$ that have an odd number of minus signs.

It is easy to check that the scalar product of two element of the same group is always an integer, so it can never be $\frac{1}{2}$. From this we deduce that two vertices in the same group are never adjacent; so this is a proper colouring.

Remark 13. There is a more algebraic way to view this colouring, since the 15 sets are the orbit of the "action" of the set $C_0 = \{\pm 1, \pm e_1, \pm e_2, \pm e_3, \pm e_4, \pm e_5, \pm e_6, \pm e_7\}$ by left-multiplication on the 240 vertices. It is important to note that C_0 is not a group, since the product is not associative.

If we equip P^8 with this colouring and perform the usual construction, we get a manifold M^8 tessellated into $2^{15} = 32768$ copies of P^8. As it was the case for P^5 and P^7, the ideal vertices have two types of behaviour. There are 2160 ideal vertices in total, 1920 of them have a 14-coloured 7-cube as a link, while the remaining 240 have a 7-coloured 7-cube. As it was the case before, 14 and 7 are respectively the maximum and minimum number of colours for a 7-cube. As usual, we can use Proposition 10 to compute the total number of cusps, which is $240 \cdot 2^8 + 190 \cdot 2 = 65280$.

Using Sage we can compute the Betti numbers of M^8:

$$b_0 = 1, \quad b_1 = 365, \quad b_2 = 33670, \quad b_3 = 583290,$$
$$b_4 = 1783226, \quad b_5 = 1346030, \quad b_6 = 456595, \quad b_7 = 65279.$$

We get $\chi(M^8) = 278528$.

1.11 Volumes

We conclude this chapter by showing the volumes of the hyperbolic manifolds $M^3, \ldots, M^8$ in Table 1.2. To compute them, we differentiate between the even and odd dimensional case. When the dimension $n = 2m$ is even, we use the Chern-Gauss-Bonnet formula

$$\mathrm{Vol}(P) = \frac{(-2\pi)^m}{(n-1)!!} \cdot \chi(P).$$

In odd dimension, we multiply the volume of the polytope P^n for the number of polytopes tessellating the manifold. In our case

$$\mathrm{Vol}(P^3) = L(2) \sim 0.91, \quad \mathrm{Vol}(P^5) = 7\zeta(3)/8 \sim 1.05, \quad \mathrm{Vol}(P^7) = 8L(4) \sim 7.92.$$

	Volume	Approx. Value	χ	Cusps
M^3	$8 \cdot L(2)$	7.28	0	3
M^4	$8\pi^2/3$	26.3	2	5
M^5	$224 \cdot \zeta(3)$	269	0	40
M^6	$512\pi^3/15$	$1.06 \cdot 10^3$	-64	27
M^7	$131072 \cdot L(4)$	$1.30 \cdot 10^5$	0	4032
M^8	$4456448\pi^4/105$	$4.13 \cdot 10^6$	278528	65280

Table 1.2: The volume, the Euler characteristic, and the number of cusps of each hyperbolic n-manifold M^n.

The symbols ζ and L indicate the Riemann and Dirichlet functions, see [50] or [21].

Chapter 2

Algebraic and Geometric Fibrations

In this chapter, we present results concerning topological and algebraic fibrations of the manifolds constructed in Chapter 1. The same results are described in [6, 29, 30].

Definition 14. An n-manifold M *fibers over* S^1 if it is a fiber bundle with base S^1. In particular, there are a $(n-1)$-manifold F and a diffeomorphism $\varphi\colon F \to F$ such that

$$M = \frac{F \times [0,1]}{(x,0) \sim (\varphi(x),1)}.$$

The manifold F is called the *fiber*, and the map φ is called the *monodromy* of the fibration. The manifold M constructed starting from F and φ is often called the *mapping torus* of the map φ.

We are particularly interested in hyperbolic manifolds that fiber over S^1. The first example of such manifold is due to Jørgersen [32] in 1977; since then, this phenomenon has been on the forefront of the study of low-dimensional topology. Thurston classified completely which surface diffeomorphisms generate mapping tori that are hyperbolic 3-manifolds, showing that those are precisely the pseudo-Anosov ones [58]. A celebrated theorem of Agol [1], together with previous results of Wise [62], shows that all closed hyperbolic 3-manifolds *virtually* fiber (i.e., each hyperbolic 3-manifold has a finite cover that fibers).

Note that, when the dimension n is even, it is impossible for a hyperbolic n-manifold to fiber. This is due to an Euler characteristic constraint, as explained below.

Proposition 15. *Let $n = 2k$ be an even positive number, and M^n be a n-dimensional hyperbolic manifold. Then, M cannot fiber over S^1.*

Proof. The Euler characteristic of any fiber bundle over S^1 always vanishes. Therefore, it is sufficient to show that $\chi(M) \neq 0$. However, it follows from the Chern-Gauss-Bonnet

Theorem that $\chi(M)$ is always proportional to the hyperbolic volume:

$$\chi(M) = (-1)^k \cdot c_n \cdot \mathrm{Vol}(M)$$

where c_n is a positive constant that depends only on the dimension n. We deduce that $\chi(M) \neq 0$, and therefore M does not fiber. □

In this case, any Morse function $f\colon M \to S^1$ must have at least $|\chi(M)|$ critical points, since the alternating sum of the numbers of critical points of each index is $\chi(M)$. We are still interested in the case of even dimension, so we generalize the concept of fibration by giving the following definition.

Definition 16. A circle-valued Morse function $f\colon M \to S^1$ is *perfect* if it has exactly $|\chi(M)|$ critical points.

When the dimension of the manifold is odd, $\chi(M) = 0$. Thus in this case a perfect Morse function is a fibration. Perfect circle-valued Morse functions for 4-dimensional manifolds have been studied in [6].

The notion of fibration can be seen also from a more algebraic point of view, by requesting a particular property that is satisfied by the fundamental group of a fibering manifold, as explained in the definition below.

Definition 17. A group G *fibers algebraically* if there is a surjective homomorphism $G \to \mathbb{Z}$ with a finitely generated kernel.

For a 3-dimensional manifold, a well-known theorem of Stallings shows that the algebraic fibering of the fundamental group is equivalent to the fibering of the manifold.

Theorem 18 (Stallings [55])**.** *If $G = \pi_1(M)$ is the fundamental group of a 3-manifold, and G fibers algebraically with kernel H, than H is the fundamental group of a surface S embedded in M, and the manifold M fibers over S^1 with fiber S.*

In higher dimension this statement is false in general, as there are recent examples of algebraic fibrations of hyperbolic manifold of dimension 4 in [3, 31], and they cannot fiber due to Proposition 15.

Despite the fact that fibrations of hyperbolic manifolds are now generally well-understood in dimension 3, not much is known when the dimension is higher. The first example of a fibering hyperbolic 5-manifold was constructed in [30], and will be explained in detail in Section 2.8.

Theorem 19. *The manifold M^5 fibers over S^1.*

All examples known so far are commensurable with M^5, and are obtained by quotienting M^5 or one of its covers. In particular, the smallest example of hyperbolic 5-manifold that is known, constructed by Ratcliffe and Tschantz in [52], fibers over the circle, and its fiber has $\chi = 1$.

2.1 A combinatorial game

In this section we review the main results of a paper by Jankiewicz, Norin and Wise [31], which is the main inspiration for our work. We wish to define some nice maps from the manifolds constructed in Chapter 1 to S^1, and we work in the piecewise linear cathegory. The manifold we are interested in are tessellated into copies of a certain right-angled polytope P, and those maps will be determined by the assignment of an appropriate *state* to each copy of P in the tessellation.

We approach this construction like a game: the initial state is allowed to change via some moves, and we win if we manage to force all the possible states to have some nice properties, that will be specified in the following sections. The prize for winning is a nice function $f\colon M \to S^1$.

2.1.1 States and system of moves

Let $P \subset \mathbb{X}$ be a right-angled polytope in some space $\mathbb{X} = \mathbb{H}^n, \mathbb{R}^n$, or S^n, with a c-colouring of its facets. A *state* for P is a partition of its facets into two subsets, denoted by I (in) and O (out). Each facet of P thus inherits a *status* I or O. We next introduce a notion to change a state for P in a controlled way.

Definition 20. A *k-system of moves* for a c-coloured polytope P is a partition of its facets into k non-empty sets $V_1, ..., V_k$ such that facets of the same colour also belong to the same set V_i. We will refer to the sets V_i as *moves*.

Given a number $i \in \{1, ..., k\}$ and a state S on P, we can apply the move i to S: the result will be a new state S' in which the I/O status of all facets in V_i is switched to the opposite status, while the other facets maintain their original status. In other words, the set V_i describes precisely which facets are inverted by the move i. We will mainly think of a system of moves as a partition of the palette of colours $\{1, ..., c\}$, and refer to $m(i)$ as the move associated to the colour i.

Let M be the hyperbolic/flat/elliptic manifold that arises from the colouring construction of Chapter 1 applied to the coloured polytope P. We now describe a procedure to propagate a state from a particular copy of the polytope P in the tessellation of M to

all the other copies of P in the tessellation. We recall that we can describe the manifold M as the simultaneous gluing of 2^c copies P_v of P, indexed by $v \in \mathbb{Z}_2^c$.

The group $\mathbb{Z}_2^c$ acts on the set of all the possible states on P in the following way. For each $i \in \{1, ..., c\}$, the element e_i acts on a state S by applying the move $m(i)$ to S; we then extend the action to every element of $\mathbb{Z}_2^c$ by linearity. To have a state on each polytope of the tessellation, it is therefore sufficient to chose an initial state S on P_0, and then propagate it to all the other copies by choosing the state $v \cdot S$ on P_v for each $v \in \mathbb{Z}_2^c$.

In most cases, we will choose the partition in moves to coincide with the partition in colours. We call this the *standard system of moves* associated to the colouring.

Remark 21. Note that in the tessellation each facet bounds two copies of P, and it has opposite status if seen in the state of the two copies of P it bounds. This is a consequence of the fact that the moves are chosen to simply be a aggregation of the partition in colours, and it will be crucial in the following sections.

2.1.2 The dual cube complex

Let $P \subset \mathbb{X}$ be a right-angled polytope in some space $\mathbb{X} = \mathbb{H}^n, \mathbb{R}^n$, or S^n, with a colouring of its facets, and let M be the resulting hyperbolic/flat/elliptic manifold. The dual of the tessellation of M into copies of P is a cube complex C. We think of C as piecewise linearly embedded in M. If P has at least one real vertex, then $\dim C = n$; otherwise, if P only has ideal vertices, C is $(n-1)$-dimensional. This fact suggests that in the hyperbolic context we should be very careful, as C is homeomorphic to M only when all vertices of P are real. When P has ideal vertices, the complement $M \setminus C$ consists of the open cusps over the ideal vertices. Therefore M retracts by deformation onto C, and C is just a spine of the manifold M; while being homotopically equivalent to M, C is not necessarily homeomorphic to it.

Each copy P_v of the polytope P corresponds to a vertex of C, which we will simply call v. Therefore, the 2^n vertices of C are indexed by $\mathbb{Z}_2^c$. The edges of C correspond to the facets of the tessellation. For each vertex v of C, and each facet F of P there is an edge connecting the vertices v and $v + e_i$, where i is the colour of the facet F. Note that the number of edges connecting v and $v + e_i$ is precisely the number of facets of P that are coloured with colour i.

Let S be a state for the polytope P_v, we notice that S induces an orientation on all the edges touching the vertex v. Consider an edge e connecting v and $v + e_i$: this edge will be dual to a facet of P, coloured with the colour i. We look at the state S in P_v, in particular at the status of the facet dual to e; if this status is I (in), we orient e as pointing inwards (towards v), otherwise, if the status is O (out), we orient e as pointing

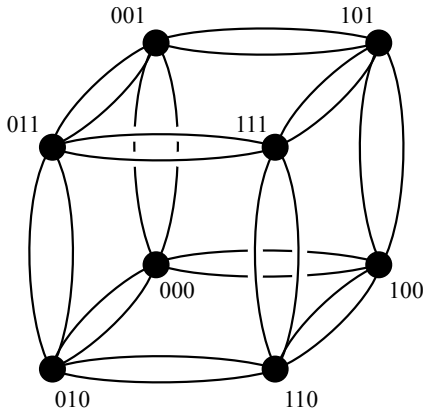

Figure 2.1: The 1-skeleton of the dual cubulation C for M^3, tessellated into 8 polyhedra P^3_v. The polyhedron P^3 is 3-coloured, and each colour is painted on two faces. The vertices of C are identified with $\mathbb{Z}_2^3$. There are two edges connecting v and $v + e_j$ corresponding to the two faces in P_v with the same colour j, for each $j = 1, 2, 3$.

outwards (towards $v + e_j$). Notice that an edge gets the same orientation from its two vertices, thanks to Remark 21, so this definition is well-posed.

An example of the cube complex C for the manifold M^3 is shown in Figure 2.1. The orientation induced by a particular state is shown in Figure 2.4.

2.1.3 Diagonal maps

We have seen in the previous section that a state on the polytope P_0 of the tessellation can be propagated to all polytopes P_v with an appropriate system of moves. Furthermore, those states induce an orientation on all the edges of the dual cube complex C. In this section, we limit ourselves to study the case in which the system of moves is the standard one, i.e., the one that coincides with the partitions of the facets in colours.

As a consequence of this choice, by construction, the orientation of the edges in C will be *coherent*, that is on every square of C (and hence on any k-cube) the orientations of two opposite edges match as in Figure 2.2. This crucial fact allows us to define a map $f\colon C \to S^1$ and directly apply Bestvina-Brady theory [9]. When the coherence condition does not hold, it is sometimes still possible to successfully define a map; this will be dealt with in Section 2.8.

The coherent orientation on the cube complex C allows us to identify every k-cube of C with the standard k-cube $[0, 1]^k \subset \mathbb{R}^k$, so that the orientations on the edges of C match the orientations of the axis in $\mathbb{R}^k$. This can be done in a unique way, up to isometries that permute the axis, but this choice will be irrelevant in the next steps. We

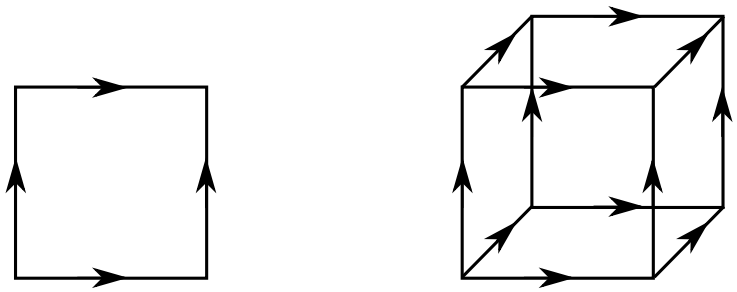

Figure 2.2: A coherent square and a coherent 3-cube: on every square, each pair of opposite edges is oriented in the same direction.

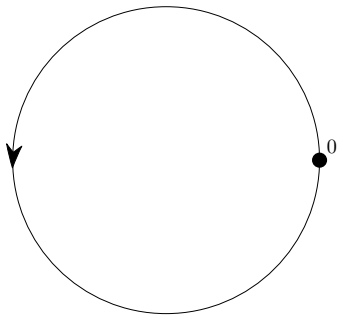

Figure 2.3: The circle S^1, seen as a cube complex with only one vertex and one edge.

can then define the diagonal map on the standard k-cube as

$$[0,1]^k \longrightarrow S^1 = \mathbb{R}/\mathbb{Z}, \qquad x \longmapsto x_1 + \cdots + x_k.$$

The diagonal maps on the k-cubes of C match to give a well-defined continuous piecewise-linear map $C \to S^1$. All the vertices of C map to the unique vertex in S^1, see Figure 2.3.

By pre-composing it with the deformation retraction $r\colon M \to C$, we finally get a *diagonal map*

$$f\colon M \to S^1.$$

From the group-theoretic point of view, the diagonal map induces a homomorphism

$$f_*\colon \pi_1(M) \to \pi_1(S^1) = \mathbb{Z}.$$

Remark 22. In the previous definition, we have assumed that the colouring and the system of moves coincide. This definition still works in a slightly more general context: one could chose a system of moves different from the colouring, but still with the property that adjacent facets are never in the same move. We call such a system a *sparse* system of moves. The coherence property for the orientation of the edges is still verified in this case, so the diagonal map could be defined in the same way.

We now show that "interesting" states actually induce "interesting" maps f_*.

Proposition 23. *Let P be a right-angled polytope, with a c-colouring that generates a manifold M. Let f and f_* be the maps induced by the choice of an initial state S on P_0. Then, one of the following holds:*

1. *In the initial state S the facets of P with the same colour also have the same status. In this case f is homotopic to a constant.*

2. *In the initial state S there are at least two facets in P with equal colour and opposite status. In this case the homomorphism $f_*\colon \pi_1(M) \to \pi_1(S^1) = \mathbb{Z}$ is non-trivial with image $2\mathbb{Z}$.*

Proof. If (1) holds, all the edges joining two given vertices of C are oriented in the same way, and we may lift the map $f\colon M \to S^1$ to a map $\tilde{f}\colon M \to \mathbb{R}$ as follows: send every vertex $v \in \mathbb{Z}_2^c$ of C to the maximum number of edges entering in v and pointing inward from distinct vertices, then extend $\tilde{f}$ diagonally to all the cubes. Since f can be lifted, it is homotopic to a constant.

If (2) holds, there are two edges joining the same pair of vertices with opposite orientation, that form a loop that is sent to ± 2 along f_*. Moreover $1 \notin \mathrm{Im}(f_*)$ because the 1-skeleton of C is naturally bipartited into even and odd vertices, according to the parity of $v_1 + \cdots + v_c$. The image $\mathrm{Im}(f_*)$ is therefore $2\mathbb{Z}$. □

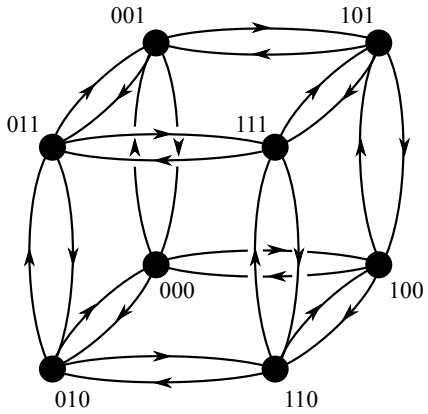

Figure 2.4: We assign a state to P^3 where faces with the same colours have opposite status. We get the orientation of the 1-skeleton of C shown here.

Case (1) is not so interesting: all the examples that we construct here on the hyperbolic manifolds M^n will be of type (2). In (2), since $\mathrm{Im} f_* = 2\mathbb{Z}$, one may decide to replace f with a lift along a degree-2 covering of S^1 to get a surjective f_*.

Corollary 24. *If all the facets of P have distinct colours, the diagonal map f is always homotopically trivial, for every choice of a state.*

This inefficient colouring is therefore useless for our purposes.

Remark 25. The result in Proposition 23 assumes that the partition of the facets of P in moves is the same as the partition in colours. In the case of the choice of a different sparse system of moves, the correct assumption to have a non-trivial map is that there are at least two facets in P with opposite status that belong to the same move. However, $\mathrm{Im}(f_*)$ could be smaller than $2\mathbb{Z}$ in this case. In this more general case, the result of Corollary 24 holds only when all the facets of P belong to different moves.

The definition of the diagonal map f depends on an initial state S on P_0. The state S induces 2^c different states on the polytopes P_v: all the states in this orbit are equivalent, as they produce the same diagonal map, up to isometries of M.

Proposition 26. *Two states S, S' that lie in the same orbit with respect to the $\mathbb{Z}_2^c$ action produce two diagonal maps $f, f' \colon M \to S^1$ that are equivalent up to some isometry of M, i.e., there is an isometry $\psi \colon M \to M$ with $f = f' \circ \psi$.*

Proof. If $S' = w \cdot S$ for some $w \in \mathbb{Z}_2^c$, we pick the isometry $\psi \colon M \to M$ that sends each polytope P_v to P_{v+w} via the identity map. It is simple to verify that we get $f = f' \circ \psi$. □

Example 27. For the 3-coloured P^3 we will choose the following state: for every pair of faces with the same colour, assign I to one face and O to the other (the choice of which face gets I and which face gets O will not affect much the result, as we will see). The resulting 1-skeleton of C is then oriented as in Figure 2.4. By Proposition 23 the homomorphism f_* is not trivial.

2.1.4 Ascending and descending links

Let P be a right-angled polytope, equipped with both a colouring and an initial state S. Let M be the manifold resulting from applying the colouring construction. As explained before, this produces a diagonal map $f\colon M \to S^1$. From Proposition 26 we have an intuition that the whole orbit of states under the system of moves plays an important role in determining the map f. We would like to study the map f, and possibly give an explicit description of it, in function of the state S.

Fortunately, a powerful machinery is already available for this task: it is Bestvina-Brady Morse theory [9]. The function f behaves like a smooth Morse function: the vertex in the cubical structure of S^1 is the only critical value. Away from the vertices of C the function glues nicely and we only have regular points. Pushing this analogy, we are going to define the *ascending and descending links* at each vertex, in order to study combinatorially those (possibly) critical points.

We first take a step back. Let Q be an Euclidean polytope dual to P. A state S on P induces a *dual state* s on Q, i.e., the assignment of a *status* I or O to each vertex of Q. We now remove the interiors of the $(n-1)$-octahedral facets from ∂Q (which correspond to the ideal vertices of P, an therefore should not be there). We are left with a flag simplicial complex $\bar{Q}$. This holds because P is right-angled, and hence simple; as a consequence, every face of Q is actually a simplex, except for the $(n-1)$-octahedral facets dual to the ideal vertices of P.

In the cube complex C dual to the tessellation of M in copies of P, the link of each vertex $v \in \mathbb{Z}_2^c$ is precisely the simplicial complex $\bar{Q}$. Since v corresponds to a particular copy of P_v, its link $\mathrm{link}(v) = \bar{Q}$ inherits a dual status on its vertices. Following [9], we highlight two subcomplexes that will be crucial in studying the behaviour of the map f near v.

We define the *ascending link* (denoted by $\mathrm{link}_\uparrow(v)$) as the subcomplex of $\bar{Q}$ generated by the vertices labelled with status O, and the *descending link* (denoted by $\mathrm{link}_\downarrow(v)$) as the subcomplex of $\bar{Q}$ generated by the vertices labelled with status I. Those complexes are completely determined by their 1-skeleton, thanks to the fact that $\bar{Q}$ is actually a flag complex.

We now consider the induced homomorphism $f_*\colon \pi_1(M) \to \mathbb{Z}$, and in particular its

kernel $H = \ker f_* < \pi_1(M)$. A theorem from [9] relates finiteness properties of H to homotopical properties of the ascending and descending links.

Theorem 28 (Bestvina-Brady [9], Theorem 4.1)**.** *Let C be an affine cell complex, with a function f defined as above, and let $H = \ker f_*$. Then:*

(i) If $\mathrm{link}_\uparrow(v)$ and $\mathrm{link}_\downarrow(v)$ are connected for every vertex v in C, then H is finitely generated, and therefore $f\colon M \to S^1$ is an algebraic fibration.

(ii) If $\mathrm{link}_\uparrow(v)$ and $\mathrm{link}_\downarrow(v)$ are simply-connected for every vertex v in C, then H is finitely presented.

As we have anticipated, when all the links are collapsible, we get a much stronger result:

Theorem 29. *Let M be a compact manifold of dimension $\dim M \leq 5$, with a decomposition as an affine cell complex C. Let $f\colon M \to \mathbb{R}/\mathbb{Z} = S^1$ be a PL Morse function, in the sense of Bestvina-Brady theory. Suppose that for each vertex $v \in C$, the links $\mathrm{link}_\uparrow(v)$ and $\mathrm{link}_\downarrow(v)$ are collapsible simplicial complexes. Then, $f\colon M \to S^1$ can be smoothed to an actual fibration.*

Proof. It suffices to show that the preimage of every closed interval with both endpoints distinct from the image of a vertex is piecewise-linearly a product. In fact, if that condition is verified, we can homotope f to be a piecewise-linear fibration. The fact that the function f can be smoothed to a fibration in the smooth cathegory follows from the fact that we are working in dimension $n \leq 5$ [28, 45].

Let $J = [a, b] \subset \mathbb{R}/\mathbb{Z}$ be such a closed interval, and let $M_J = f^{-1}(J)$. If no images of a vertex are contained in J, then the manifold M_J is simply a union of prisms. Therefore M_J is PL homeomorphic to the product manifold $M_a \times J$, where $M_x \colon = f^{-1}(x)$.

Let v be a vertex of C, and let $t = f(v) \in \mathbb{R}/\mathbb{Z}$ be the image of v. Take $J = [t - 2\varepsilon, t + 2\varepsilon]$ to be a small interval such that t is the only value that is image of a vertex. We first assume, for the sake of simplicity, that v is the only vertex that is mapped to t. Then [9, Lemma 2.5] shows that the manifold $M_{[t-2\varepsilon,t+\varepsilon]}$ collapses onto $M_{[t-2\varepsilon,t-\varepsilon]} \cup C_v$, where we have coned off the descending link $\mathrm{link}_\downarrow(v)$ with the cone C_v. Since $\mathrm{link}_\downarrow(v)$ is collapsible, then the manifold $M_{[t-2\varepsilon,t+\varepsilon]}$ collapses onto $M_{[t-2\varepsilon,t-\varepsilon]}$, and therefore $M_{[t-\varepsilon,t+\varepsilon]}$ is PL homeomorphic to the product $M_{-\varepsilon} \times [-\varepsilon, \varepsilon]$. If more vertices are mapped to t, we can apply the same argument separately to all of them, since everything is performed locally. This yields the theorem. □

When the dimension is even we cannot have a fibration, as we have seen in Proposition 15. It is still interesting to investigate whether the constructed function has the minimal number of critical points. A different version of Theorem 29 still holds.

Theorem 30 ([6], Theorem 15)**.** *Let P be a 4-dimensional polytope, and let M, C, and $f\colon M \to \mathbb{R}/\mathbb{Z} = S^1$ as above. Suppose that at every vertex v both the links $\mathrm{link}_{\uparrow}(v)$ and $\mathrm{link}_{\downarrow}(v)$ collapse to a connected polyhedron of dimension ≤ 1, and to a point if v is a boundary vertex. Then $f : M \to S^1$ can be smoothed to a Morse function with only critical points of index 2.*

Theorem 29 and Theorem 30 require the manifold M to be compact. In particular, they are not directly applicable to manifolds that are built using a hyperbolic polytope P which has some ideal vertices. To do that, we need to use a truncated version of P, in which the cusps are cut along some horospheres. This is explained in detail for the 5-dimensional manifold M^5 in Section 2.8.

In the simpler case of the manifolds of dimension 3 and 4, we avoid this truncation procedure, and look only for the critical points in the cube complex generated by the construction that uses P. Although this is not completely precise, hiding these technicalities allows us to keep the focus on the main conditions for the construction. A more complete exposition in this regard can be found in [6] and [43].

Finally, the proof of Theorem 30 given in [6] can be adapted to work also to 6-dimensional polytopes; obtaining only critical points of index 3. However, this generalization will not be used in this thesis.

2.1.5 Additional terminology

We introduce some terminology, mainly following [31] and [29].

Let P be a right-angled polytope, together with a c-colouring and an initial state. After propagating such state with the standard system of moves, we end up with an orbit of 2^c different states, from which we can deduce the ascending and descending links of the critical points of the function $f\colon M \to S^1$.

We say that a state S for P is *legal* if the ascending and descending links of that states are both connected simplicial complexes. We say that the orbit is *legal* if all states in that orbit are legal. The objective of the combinatorial game introduced in [31] is precisely to find a legal orbit. If an initial state generates a legal orbit, Theorem 28 ensures that the function f is an algebraic fibration.

Following [29], we slightly generalize the previous concept, saying that a state S is *1-legal* if the ascending and descending links of that states are both simply connected. Analogously, an orbit is *1-legal* if all states in that orbit are 1-legal. As a consequence of Theorem 28, if an initial state generates a 1-legal orbit, than the kernel H of the homomorphism $f_*\colon \pi_1(M) \to \mathbb{Z}$ is finitely presented.

Finally, we give the following definition.

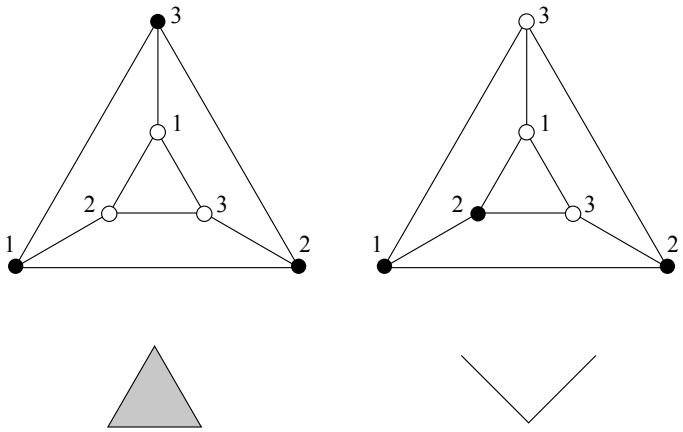

Figure 2.5: The dual of P^3 is a triangular prism, with the lateral squares removed. We exhibit a state by colouring the vertices in black and white, with black (white) corresponding to the status I (O). There are only two states in the orbit of P^3 up to isomorphism, and in both cases the ascending and descending links are contractible: they are a triangle and two segments joined along an endpoint.

Suppose that the number of facets of a particular colour is always the same even number $2m$. We say that a state S on P is *balanced* if for every colour, the number of facets labelled with the status I is the same as the number of facets labelled with the status O. If we choose the standard system of moves associated to the colouring, and we propagate a balanced state, it is easy to show that all the states in the orbit maintain the property of being balanced. For this reason, balanced states are often a wonderful choice, since they coordinate well with all the symmetries of our polytopes, drastically reducing the number of isomorphism classes of links that come into play.

2.2 A fibration for the manifold M^3

We recall that the manifold M^3 was constructed starting from the 3-colouring of the polytope P^3 shown in Figure 1.7. We now assign an initial state to P^3 in the following way: for every pair of facets that share a colour, we assign the status I to one of them, and the status O to the other one. In this way we get a balanced state. With the standard system of moves associated to the colouring, the orbit of states consists of precisely all the $2^3 = 8$ balanced states. Up to isomorphism, we find that those 8 states reduce to only 2 classes, both shown in Figure 2.5. In both cases, the ascending and descending links are all collapsible to a point. Moreover, the states that are inherited by the sections of the cusps can be seen by looking at the three lateral squares of Figure

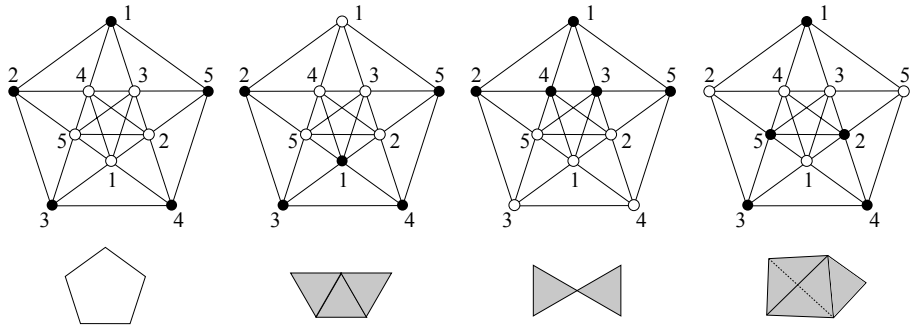

Figure 2.6: The dual of P^4 is the Gosset polytope 0_{21}. We exhibit a state by colouring the vertices in black and white, with black (white) corresponding to the status I (O). There are only four states in the orbit of P^4 up to isomorphism. In the first case both the ascending and descending links are circles, and they form an Hopf link. In all other cases we always get a collapsible link; we only show the descending link, the ascending links are of the same type.

2.5. In all cases, both ascending and descending links are collapsible. We deduce that the diagonal function $f\colon M \to S^1$ satisfies the conditions of Theorem 28 and therefore it can be smoothed to a fibration.

2.3 A perfect Morse function on M^4

We recall that the manifold M^4 was constructed starting from the 5-colouring of the polytope P^4 shown in Figure 1.10. As it was in the case of P^3, each colour involves a pair of facets. We can assign an initial state to P^4 in the same way we had done for P^3: we arbitrarily chose a balanced state. Propagating this state with the standard system of moves associated to the colouring, we obtain as an orbit precisely the $2^5 = 32$ states that are balanced. Up to isomorphism, we find that those 32 states reduce to only 4 classes, shown in Figure 2.6. In 2 out of 32 states we get the picture on the left, where both ascending and descending links are circles, and if we consider them embedded in the boundary of the Gosset polytope 0_{21}, they form a Hopf link in S^3. In all the other 30 states, both links are collapsible. Corresponding to the 5 ideal vertices of P^4, there are 5 cubes that tessellate the cusps of M^4. By looking at Figure 1.11, one could see that such cubes have a pair of facets with the same colour. Since our states are balanced, those two facets will inherit opposite states. We deduce that both the ascending and descending links will be cones on those two points, and therefore they are collapsible. In particular, the restriction to the cusps of the function f is a fibration. The conditions in Theorem 30 are hence verified, so the diagonal function $f\colon M^4 \to S^1$ can be smoothed

to a perfect circle-valued Morse function, having two index-2 critical points.

From the algebraic point of view, we have obtained that the kernel H of the homomorphism $f_*\colon \pi_1(M^4) \to \mathbb{Z}$ is finitely generated; since all ascending and descending links are connected. The map f is therefore an algebraic fibration.

2.4 A perfect Morse function from the 24-cell

We recall that we had selected a colouring for the 24-cell in Example 8. We now describe a legal state for it, following [6]. We use the quaternionic description of the vertices of the 24-cell, keeping in mind that the polytope is self-dual. We had divided the vertices into 3 octets: $\pm 1, \pm i, \pm j, \pm k$, the ones of type $\frac{1}{2}(\pm 1 \pm i \pm j \pm k)$ with an even number of minus signs, and those with an odd number of minus signs. Such subdivision was exactly the subdivision in orbits of the action of the group $G = \{\pm 1, \pm i, \pm j, \pm k\}$ by left multiplication on the vertices.

We now consider the subgroup $H = \{\pm 1, \pm i\} < G$, and its action by left multiplication on the vertices. Each of the monochromatic octects is subdivided by the action of H into orbits of 4 elements each. We chose an initial state S by assigning arbitrarily the status I to one orbit, and the status O to the other one. As we have already noted in the previous cases, the state is balanced; and this property is maintained with the propagation. The orbit under the standard system of moves therefore consists of all the states obtainable with the 8 different possible choices for S.

All the states in the orbit are actually isometric, and thus generate the same ascending and descending links. Such link are two annuli, and form together a (banded) Hopf link in S^3, if viewed inside the boundary of the 24-cell. Moreover, one could verify in the same way that the links of ideal vertices inherit states that produce collapsible ascending and descending links. The conditions in Theorem 30 are hence verified, so the diagonal function $f\colon M^4 \to S^1$ can be smoothed to a perfect circle-valued Morse function, having eight index-2 critical points.

2.5 A legal orbit for M^6

In the 9-colouring for P^6 the 27 facets are partitioned into 9 triplets. As opposite to the previous cases, it is not possible to chose a balanced state here. Furthermore, there is no obvious choice that plays well with the symmetries off P^6. However, a brute force computer search shows that there are many legal orbits for P^6. For instance, we may take S as the state where the first vertex in each triple listed in Section 1.8 is O and the remaining two are I. By using our Sage program we find that the orbit of this state

is legal. By Theorem 28 the kernel H of $f_*\colon \pi_1(M^6) \to \mathbb{Z}$ is finitely generated.

As we said, a computer search shows that many initial states S yield legal orbits. However, no 1-legal orbits were found with this method.

With a more refined argument, using a non-standard system of moves (and a different colouring of P^6), one could build a different manifold N^6 with a map $g\colon N^6 \to S^1$ that is a perfect Morse function. This also yields a 1-legal orbit, and therefore the kernel H of $g_*\colon \pi_1(N^6) \to \mathbb{Z}$ is finitely presented. The manifold N^6 is commensurable with M^6, since the manifold produced by the 27-colouring of P^6 finitely covers both of them. This theorem is joint work with Migliorini, and is currently in preparation. Some details of the proof can be found in [43].

2.6 A 1-legal orbit for M^8

The combinatorics of the polytope P^8 is much more complicated than all previous examples. Having 240 facets, there are 2^{240} possible states that can be chosen. Moreover, we are using a colouring that uses 15 colours. Assuming we use the standard system of moves associated to the colouring, the orbit will consist of $2^{15} = 32768$ states, and we need *all of them* to be legal.

To accomplish this task, we will once again let the construction for the 24-cell be of inspiration; and hope that the beautiful symmetries of P^8 will substantially reduce these numbers.

We recall that the dual polytope to P^8 is the Gosset polytope 4_{21}. As we had already done to choose a colouring in Section 1.10, we see it embedded in the octonion space $\mathbb{O}$, and we recall that the colouring was a partition in 15 hextets, that is $\{\pm 1, \pm e_1, \pm e_2, \pm e_3, \pm e_4, \pm e_5, \pm e_6, \pm e_7\}$, the elements $\frac{1}{2}(\pm 1 \pm e_n \pm e_{n+1} \pm e_{n+3})$ and $\frac{1}{2}(\pm e_{n+2} \pm e_{n+4} \pm e_{n+5} \pm e_{n+6})$ with an even number of minus signs, and those with an odd number of minus signs, with the integer n varying modulo 7. This colouring came from the "action" of $O = \{\pm 1, \pm e_1, \pm e_2, \pm e_3, \pm e_4, \pm e_5, \pm e_6, \pm e_7\}$ on the vertices, in a similar way to the colouring for the 24-cell, that came from the action of $\{\pm 1, \pm i, \pm j, \pm k\}$ on the vertices. Even though the non-associativity of octonions makes this analogy somewhat flawed, we can still push it a bit further to define a state.

The definition of a state on the 24-cell came from the restriction to the action of the subgroup of the complex numbers $H = \{\pm 1, \pm i\}$ on the vertices; the natural analogous on the octonions would be to consider the subset of quaternions $Q = \{\pm 1, \pm e_1, \pm e_2, \pm e_3, \pm e_4\} \subset O$ and its action on the vertices. Unfortunately, this is not really a group action because octonions are not associative, and hence we may have that $e_1(e_2(x)) \neq (e_1 e_2)(x)$. Therefore some caution is needed. To circumvent this problem,

we chose a privileged representative inside each hextet:

$$1 \in C_0, \qquad 1 + e_n + e_{n+1} + e_{n+3} \in C_n^+, \qquad -1 + e_n + e_{n+1} + e_{n+3} \in C_n^-$$

where n runs modulo 7.

We are now ready to select the initial state S on 4_{21}. For each one of those 15 representatives, we consider the 8 vertices that can be obtained by left-multiplying the representative for elements of Q, and assign to all of those the status O; we assign the status I to all the remaining vertices. In this way, the state S is balanced, and thus its orbit will consist of 2^{15} balanced states.

We now need to determine the ascending link and descending link for each one of the states in the orbit, and we end up with $2 \cdot 2^{15} = 65536$ graphs to analyse (as we have previously mentioned the 1-skeleton determines the whole link, since it is a flag complex). To do this, we have used our Sage code, and discovered that those graphs reduce to only 185, up to isomorphism. Furthermore, our Sage program certifies that each one of the generated simplicial complexes is connected and simply connected; therefore the orbit is 1-legal.

We deduce from Theorem 28 that the map $f\colon M^8 \to S^1$ is an algebraic fibration, and furthermore that the kernel H of $f_*\colon \pi_1(M^8) \to \mathbb{Z}$ is finitely presented.

Remark 31. The function f is not a perfect circle-valued Morse function. In fact, some of the states generate some links that are wedges of more than one sphere.

2.7 A 1-legal orbit for M^7

In the 14-colouring for P^7 the 56 facets are partitioned into 14 quartets. The colouring came from the colouring of P^8, so we are going to do the same thing for the states. We see P^7 as the facet of P^8 dual to the vertex 1 in 4_{21}. The state S that we chose for P^8 in the previous section induces a state S' for P^7 in a natural way: every facet of P^7 inherits the status of the adjacent facet in P^8.

As in all previous cases, the state S' is balanced, and thus the whole orbit of states will be balanced. The orbit of consists of 2^{14} states, each contributing with their ascending and descending link. Using Sage we are pleased to discover that the resulting $2^{15} = 32768$ graphs reduce to only 106 up to isomorphism. Once again, balanced states together with the many symmetries of the considered polytope drastically reduce the number of graphs involved.

Using Sage we also see that all the simplicial complexes generated by the 106 graphs are connected and simply connected. Therefore the orbit is 1-legal. All the data can be found in [63]. By Theorem 28 the map f is an algebraic fibration, and the kernel H of $f_*\colon \pi_1(M^7) \to \mathbb{Z}$ is finitely presented.

Remark 32. In our examples in dimension $n = 3, 4$ the construction via the diagonal map provided orbits that satisfy the conditions of Theorem 29 and Theorem 30. This fact allowed us to smoothen f to be a fibration or a perfect circle-valued Morse function, depending on the dimension. Our choice of state for P^7 looked pretty lucky, but one may wonder whether it is possible to get even luckier and obtain a fibration for M^7 with another initial state. Unfortunately, the next proposition shows that this is not possible: the restriction of the diagonal map to one of the cusps will always be an obstruction.

Proposition 33. *For any possible choice of an initial state on P^7, there is some cusp $X \cong T^6 \times [0, +\infty) \subset M^7$ where the restriction $f|_X$ is homotopic to a constant. In particular, f is not homotopic to a fibration.*

Proof. Let S be any initial state for P^7. In our discussion in Section 1.9 we noticed that there is an ideal vertex v of P^7 whose link C is a 6-cube coloured with 12 distinct colours. Let $T \subset M^7$ be a torus section that lies above C. The restriction of f to T is determined by the restriction of the state S of P^7 to T. By Corollary 24 the restriction of f to T is homotopically trivial, and hence it is so on the cusp $X = T \times [0, +\infty)$ that it bounds. Since f is homotopic to a constant when restricted to a cusp, it cannot be a fibration. □

2.8 A fibration for M^5

The argument we presented in Proposition 33 holds also for the colouring chosen for M^5. We recall that M^5 has 40 cusps in total, that we had classified in two types. The one we called the small cusps are the one above 8 ideal vertices of P^5 whose link were 4-coloured 4-cubes, and are 32 in total. The remaining 8 cusps, that we called large cusps, are above the remaining 2 ideal vertices, and their link was an 8-coloured 4-cube. As it happened for M^7, if we build a diagonal map f generated by the standard system of moves associated to the colouring, the restriction to the large cusps will necessarily be homotopic to a constant. More in general, it turns out that *any* choice of a colouring and of a sparse system of moves has this property. Therefore, it is impossible to construct a fibration with the techniques we have described up to this point. To get around this problem, we need to generalize the theory in order to define and study a function f even when the system of moves is not sparse. For the sake of simplicity, we are going to describe our theory in the specific case of P^5 instead of the general case.

2.8.1 The truncated polytope

The manifold M^5 is diffeomorphic to the interior of a compact manifold $\overline{M}^5$. The 40 cusps of M^5 correspond to 40 boundary components of $\overline{M}^5$, each homeomorphic to a 4-torus. We are going to describe the manifold $\overline{M}^5$ by gluing copies of $\overline{P}^5$, a truncated version of the polytope P^5.

Consider P^5 as an Euclidean polytope in $\mathbb{R}^5$, as described in Section 1.7. Let $\overline{P}^5$ be the truncated P^5, that is, the polytope obtained from P^5 by intersecting it with the 10 half-spaces of equation

$$x_i \leq 1 - \varepsilon, \quad x_i \geq -1 + \varepsilon;$$

for some fixed small $\varepsilon > 0$. In other terms, we have removed from P^5 some small neighbourhoods of the ideal vertices.

The polytope $\overline{P}^5$ has 26 facets; 16 of those are the truncation of the facets of P^5 and are truncated version of P^4, while the 10 new facets produced by the truncation of the ideal vertices are some 4-cubes. From this, we see that $\overline{P}^5$ has $176 = 16 + 16 \cdot 10$ vertices: in addition to the 16 original real vertices, we also have the vertices of the 10 new hypercubes.

The colouring chosen for P^5 in Section 1.7 can be applied also to $\overline{P}^5$; we simply choose the same colouring, leaving the 10 hypercubes uncoloured. We can then perform the usual gluing procedure, taking 2^8 copies of $\overline{P}^5$ and gluing them as prescribed by the colouring. The uncoloured hypercubes are left unglued, and their union forms the boundary of the resulting manifold $\overline{M}^5$. It is easy to verify that the interior of the manifold $\overline{M}^5$ is actually homeomorphic to M^5.

We now want to construct a cubulation $\overline{C}$ for the manifold that is the correspondent to the cubulation C dual to the tessellation of the manifold M^5. Analogously to the original case, we start from the tessellation of $\overline{M}^5$ into 2^8 copies of $\overline{P}^5$. We then fix a baricentric subdivision for the polytope $\overline{P}^5$, and lift it to a baricentric subdivision of the tessellation. We consider all the vertices that are in the original (not subdivided) tessellation of $\overline{M}^5$, and notice that there are vertices of two types: those that are on the boundary, and those who are in the interior. Given a vertex v, we are interested in its star $St(v)$, that is of two types, depending on the type of v:

- If v lies in the interior of $\overline{M}^5$ (which means that v corresponds to one of the 16 vertices of P^5), then $St(v)$ is the baricentric subdivision of a 5-cube having v as a center. This is due to the fact that P^5 is right-angled.

- If v lies on the boundary of $\overline{M}^5$, then v corresponds to one of the additional 160 vertices of $\overline{P}^5$ that came from the truncation. The star $St(v)$ is one half of the baricentric subdivision of a 5-cube, with v at the center of the cube.

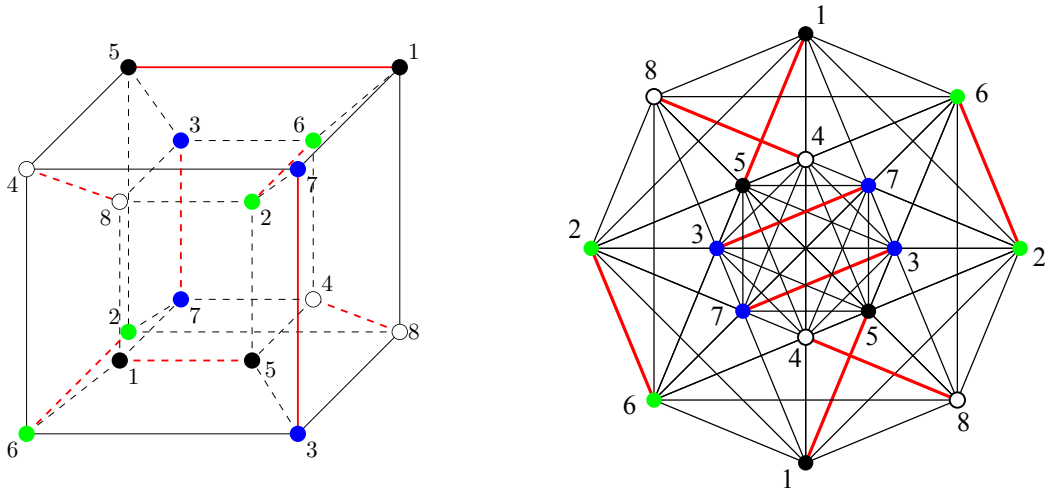

Figure 2.7: The four moves of the system, depicted with four different colours. Each move is subdivided into two pairs of adjacent facets. The adjacencies are indicated here as red edges. As usual, we show both models for P^5. In the picture on the left, two vertices are adjacent if they are connected by a path of lenght ≤ 2. In the picture on the right, some edges are superposed.

We now consider all the 5-cubes obtained in this way (considering that half of a 5-cube is still a 5-cube), and notice that they intersect only along common facets, and that those intersections are dual to the edges of the tessellation of $\overline{M}^5$. This decomposition in cubes is therefore a cube complex $\overline{C}$, which is PL-isomorphic to the manifold $\overline{M}^5$.

2.8.2 A system of moves

We have coloured P^5 with a palette of 8 colours $\{1, 2, 3, 4, 5, 6, 7, 8\}$. To define a system of moves, we pair up this 8 colours into 4 pairs. Each move will therefore consist of 4 facets of P^5. Here is the subdivision:

$$\mathcal{S} = \big\{\{1, 5\}, \{2, 6\}, \{3, 7\}, \{4, 8\}\big\}.$$

A picture of this subdivision is shown in Figure 2.7. This system of moves is not sparse, since there are 8 pairs of adjacent facets that belong to the same move.

As initial state, we choose the one in Figure 2.8. It is a balanced state in the usual sense: each colour (and thus each move) has the same amount of vertices with status I and status O.

We can now propagate the initial state S using the system of moves $\mathcal{S}$ to all the 256 copies of P^5 that tessellate M^5, and we get $2^4 = 16$ different states. As prescribed by our procedure, we now look at the cube complex C that is dual to the tessellation, and use the states to orient all the edges of C. Here we clash with the consequences of having

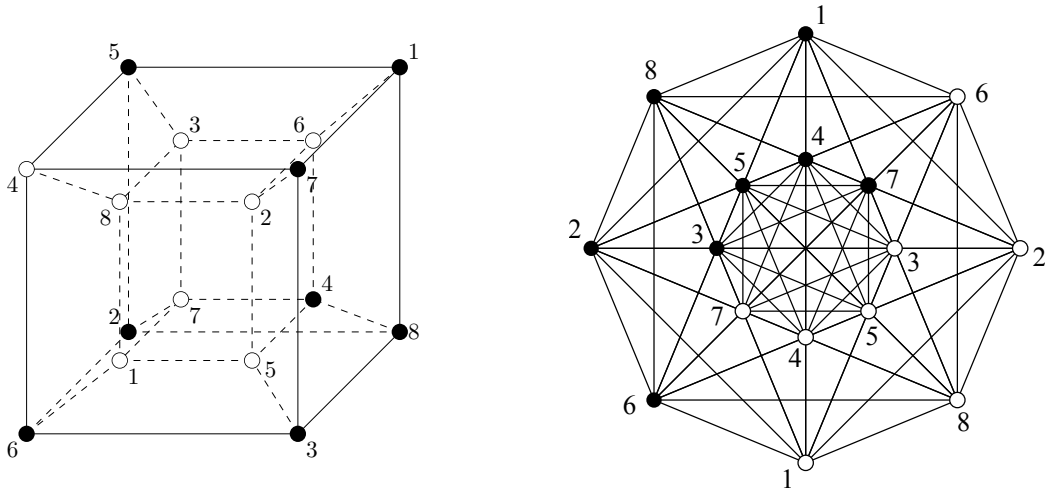

Figure 2.8: The chosen initial balanced state S for P^5. The black (white) dots indicate the status I (O). We show both models for P^5. As usual, in the picture on the left, two vertices are adjacent if they are connected by a path of lenght ≤ 2. In the picture on the right, some edges are superposed.

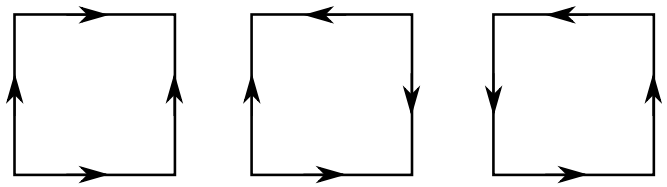

Figure 2.9: Three types of squares with oriented edges. The first is oriented coherently. Square of the second type arise in the cube complex C, in correspondence of the bad ridges. The third type of square is not present in C.

chosen a system of moves that is not sparse: the orientation of C is not coherent. In fact, there are squares oriented in a way such that both opposing pairs of sides have the opposite orientation (see Figure 2.9). Following the terminology of [30], we call those *bad squares*.

Our goal is now to define a map f from C to S^1, in a similar way of what was done when the orientation of C was coherent. To do this, we are going to subdivide the cube complex C.

Before doing that, we briefly look into the states in the orbit we have chosen.

Proposition 34. *For all states of the orbit, both the ascending and descending links are collapsible.*

Proof. All the 16 states in the orbit are actually isomorphic. To prove that the links

are collapsible, it suffices to show that there is a vertex x that is connected to all other vertices. In fact, since the links are flag simplicial complexes, x would be contained in every maximal simplex; and the whole link would collapse to x. To show that such a vertex x exists in every link, we look at the representation of the 1-skeleton of 1_{21} as a 4-cube, as in Figure 2.8-(left). The vertices that have status I (or O) are always arranged in a particular way: seven of them are the vertices of a 3-cube that is a facet of the 4-cube, while the last one is the vertex that is opposite (in the 4-cube) to the remaining spot of the 3-cube. In such an arrangement, the vertex that is opposite (in the 3-cube) to the empty spot of the 3-cube is always adjacent to all the other ones. For instance, if we look at all the black points in 2.8-(left), they occupy seven positions in the outside 3-cube. The vertex coloured with the colour 8 is the one adjacent to all the others. □

As an effect of the truncation of P^5, the extended cube complex $\overline{C}$ has some more vertices, laying on its boundary and corresponding to ideal vertices of P^5. The link of an ideal vertex of P^5 is a 4-cube, and it inherits a state from P^5 in the same way it inherits a colouring. As we have seen, the boundary of M consists of 40 copies of 4-tori, tessellated in some copies of those 4-cubes. The inherited states on the cubes define a function on ∂M, that will coincide with the restriction of f. To analyse it, we can look at the ascending and descending links of the vertices of the cube complex representing ∂M. Such links are subcomplexes of a 4-octahedron dual to the 4-cube.

Proposition 35. *For all states in the orbit, the ascending and descending links at every ideal vertex of P^5 are collapsible.*

Proof. We use again the representation of the 1-skeleton of 1_{21} as a 4-cube as in the left part of our pictures. We recall that there are 10 octahedral facets in total, dual to the ideal vertices of P^5. Eight of those octahedral facets 1_{21} correspond to the eight 3-cubes that are facets of the 4-cube; while the remaining two correspond to the vertices coloured with colours 5, 6, 7 and 8, and to the vertices with colours 1, 2, 3, 4. As it can be seen from Figure 2.7-(left), in each one of those 4-octahedra there is a pair of opposite vertices that have opposite status. Such vertices are adjacent to all the other vertices that have their same status, so the two links collapse on those vertices. □

2.8.3 The subdivided cell complex

As we have seen, the induced orientation on the edges of the cubulation of $\overline{M}^5$ will contain some bad squares like in Figure 2.9-(center or right) and there is no way to define on such a square an affine function that is coherent with the orientation of the

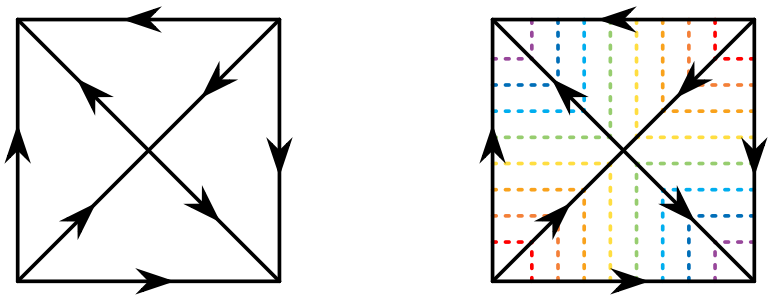

Figure 2.10: A subdivision of a bad square into four triangles. On each triangle there is a natural affine height function inducing the orientation of its edges. Some level set of those functions are shown on the right: it looks like a piecewise linear saddle point.

edges. We circumvent this problem by subdividing the cube complex into smaller pieces: we cut all the cubes that contain these bad squares into four prisms.

We first determine the bad squares. Recall that a ridge in P^5 is a 3-dimensional face. We call a ridge *bad* if the colours of the adjacent facets belong to the same move. The 8 bad ridges of P^5 are thus dual to the 8 red edges shown in Figure 2.7. The bad squares contained in the interior of $\overline{M}^5$ are precisely those that are dual to some 3-stratum that projects to a bad ridge of P^5. In our initial state, the statuses of the two facets incident to a bad ridge coincide, so this is still true in all other states. Therefore, the bad square is as in Figure 2.9-(center) and not as in Figure 2.9-(right). The other bad squares in $\overline{M}^5$ are those contained in the boundary that are parallel to some interior bad square through a 3-cube. As expected, those are identical to their copy in the interior.

The only bad squares are thus as in Figure 2.9-(center). To define a function f on these squares, we notice that they can be subdivided into four triangles as in Figure 2.10-(left). On each triangle T there is a natural affine height function $T \to \mathbb{R}/\mathbb{Z}$ that induces the orientation of its edges and sends the three vertices to $0, \frac{1}{2}$, and $1 = 0$ (it is just the coordinate in the direction of the corresponding side of the square). The four affine functions match along the edges and the central vertex of the bad square is sent to $\frac{1}{2}$ (as a kind of piecewise-linear saddle point). The level sets of such functions are shown in Figure 2.10-(right).

We now look into the bigger picture, analysing how bad squares sit into higher-dimensional cubes. Luckily for us, bad ridges are sufficiently far from each other in P^5 to avoid forming 4-cubes that are products of bad squares. Given two cubes C, C' with oriented edges, there is a natural way to orient all the edges of $C \times C'$, since these are either of the form $e \times \{p'\}$ for some edge $e \subset C$ or of the form $\{p\} \times e'$ for some

edge $e' \subset C'$. A product of cubes with coherent orientations is a cube with coherent orientation.

A k-cube of the cubulation of $\overline{M}^5$ is called *good* if it is coherently oriented and *bad* otherwise. We already know that $\overline{M}^5$ contains only one type of bad squares. More generally, we now prove there is only one type of bad k-cubes for every $k \geq 2$.

Proposition 36. *Every k-cube of the cubulation of $\overline{M}$ is oriented either coherently, or as $C \times C'$ for some bad square C and a coherently oriented $(k-2)$-cube C'.*

Proof. This holds because the bad ridges in P^5 are pairwise disjoint. This can be proved by checking that all the cliques in Figure 2.7 contain at most one red edge. □

We now subdivide the cube complex decomposition of $\overline{M}$ by cutting each bad k-cube $C \times C'$ into four prisms $T \times C'$, where T is one of the four triangles contained in the bad square C as in Figure 2.10.

This results in a new affine cell decomposition of $\overline{M}$, in which all the edges are oriented. All the affine cells have a natural affine function that is compatible with the edges orientations: we have already defined it on the triangles and the edges, and we can extend it to a diagonal map on all the products. These affine functions all match to a circle-valued Morse function $f\colon \overline{M} \to \mathbb{R}/\mathbb{Z}$.

The function f has two (possibly) critical values (0 and $\frac{1}{2}$). The value 0 corresponds to original the vertices of the cubes, while the value $\frac{1}{2}$ corresponds to the new vertices introduced in our subdivision, that are now also (possibly) critical points. To prove that f is a fibration, we now look into all these (possibly) critical points, and prove that all ascending and descending links are collapsible.

Theorem 37. *The ascending and descending links at all the vertices of the affine cell decomposition are collapsible polyhedra. Therefore f is homotopic to a fibration.*

Proof. There are 3 types of vertices w in the affine cell decomposition:

1. the barycenters of some polytope $\overline{P}^5_v$,
2. the barycenters of some 4-cube facet of $\overline{P}^5_v$, that lie in $\partial\overline{M}^5$,
3. the barycenters of the bad squares.

The vertices of type (1) and (2) are those of the original cubulation, while those of type (3) were introduced in the subdivision into prisms. We analyse the three cases separately. The collapsibility of the ascending and descending links of the vertices of type (1) and (2) is deduced by the collapsibility of the links in the orbit of states of P^5; however, we need to add some further comments to Proposition 34 and Proposition

35 to address the subdivisions. For the vertices of type (3), the collapsibility follows essentially from Figure 2.5. Here are the details.

We start with (1). Let w be the barycenter of $\overline{P}^5_v$. Its link $\mathrm{link}(w)$ in the affine cell decomposition is the boundary of the Gosset polytope 1_{21}, with a couple of further subdivisions:

(i) the 4-octahedra dual to the ideal vertices of P^5 are each subdivided into 16 simplexes by adding a central vertex (which indicates an edge pointing towards a vertex of type (2));

(ii) one additional vertex is added at the barycenter of each edge dual to a bad ridge of P^5_v, and all the adjacent simplexes are subdivided in two (the additional vertex indicates an edge pointing towards a vertex of type (3)).

Recall from Proposition 34 that the ascending and descending links of the state S_v are some collapsible subcomplexes of the complex K obtained from the boundary of 1_{21} by removing its 4-octahedra. Note that $\mathrm{link}(w)$ is obtained from K by adding and subdividing some simplexes (these are the modifications (i) and (ii) described above). The ascending and descending links of w in $\mathrm{link}(w)$ are obtained from those of S_v by the following corresponding modifications:

(i) the central vertex of each 4-octahedron has status O because the edges of the cubulation that intersect the boundary in one endpoint are directed towards it by construction; the central vertex is hence added to the ascending link, together with all the simplexes containing it spanned by vertices with status O; by Proposition 35, the link of this new central vertex in the ascending link is collapsible, so this operation is an expansion (the new ascending link collapses onto the old one);

(ii) some simplexes are subdivided, but this does not change the piecewise-linear homomorphism type of the ascending and descending links.

The ascending and descending links of S_v are collapsible by Proposition 34, so the resulting ascending and descending links at w also are collapsible, and this concludes the proof for Case (1).

We turn to (2). Let $w \in \partial\overline{M}^5$ be the barycenter of a boundary 4-cube facet of some polytope $\overline{P}^5_v$, which corresponds to an ideal vertex of P^5. The link $\mathrm{link}(w)$ of w in the decomposition is a cone over a polytope that is a 4-octahedron with some further subdivisions at the edges dual to the bad ridges. The parts of the ascending and descending links contained in the subdivided 4-octahedron are collapsible by Proposition

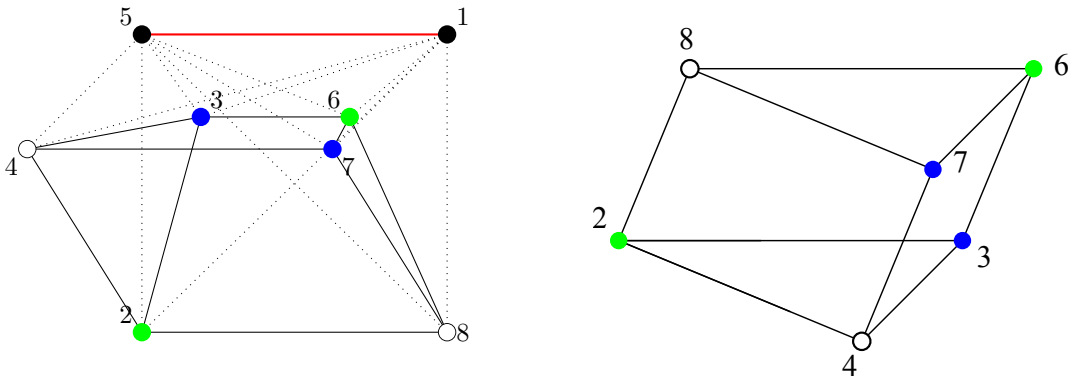

Figure 2.11: The 6 other facets incident to the top bad ridge adjacent to two facets with colour 1 and 5. We show a picture for each of the models of 1_{21}, both pictures are subgraphs of Figure 2.7.

35. The vertex of the cone has status I, so the descending link is further modified by some expansion. Therefore the ascending and descending links at w are collapsible.

Finally, we examine the case (3). Let w be the barycenter of some bad square. This can lie either in the interior or in the boundary of $\overline{M}^5$. If it lies in the interior, it is dual to a 3-stratum that projects to a bad ridge of P^5. The link link(w) of w in the decomposition is the join of a square (dual to the bad square) and a triangular prism (dual to the ridge). The square has vertices with status I,O,I,O, as one can deduce from Figure 2.9-(center). The triangular prism has the status inherited from the bad ridge.

By looking carefully at Figure 2.7 we deduce that a bad ridge that is the intersection of two facets with colours $t, t+4$ is also incident (along its 6 triangular faces) to facets of all the other 6 colours, whose statuses can be as in Figure 2.5. For instance, the 6 facets one obtains from the top-left bad ridge incident to the facets coloured with 1 and 5 are shown in Figure 2.11. Since the ascending and descending links in Figure 2.5 are collapsible, they remain so after the join with two vertices with status I (or O).

If the bad square lies in $\partial\overline{M}^5$, the link of w is the cone over the join of the square with vertices I,O,I,O and another square, which is one of the three square faces of the prism shown in Figure 2.5. In all the cases shown in the figure the square face contains contractible ascending and descending links and hence we conclude as above. □

Theorem 19 is therefore proved.

2.8.4 The restriction to the boundary

The fibration $f\colon M^5 \to S^1$ restricts to a fibration in each of the 40 boundary 4-tori. To analyse these restrictions, we need to distinguish again between large and small cusps.

We recall that the decomposition of $\overline{M}^5$ into copies of $\overline{P}^5$ induces a decomposition of $\partial\overline{M}^5$ into 4-cubes. The 32 small cusps correspond to 32 small boundary tori, that decompose as $2\times2\times2\times2$ hypercubes. We identify each one of them with $\mathbb{R}^4/2\mathbb{Z}^4$. The 8 large cusps correspond to 8 large boundary 4-tori, and decompose as $4\times4\times4\times4$ hypercubes. We identify each one of them with $\mathbb{R}^4/4\mathbb{Z}^4$.

Proposition 38. *The fibration, when restricted on the cusps of M^5, can be of two types:*

(i) If the cusp is one of the 32 small cusps; then the fibration is isotopic to a map of type $f(x_1,x_2,x_3,x_4)=x_1+x_2+x_3+x_4$.

(ii) If the cusp is one of the 8 large cusps; then the fibration is isotopic to a map of type $f(x_1,x_2,x_3,x_4)=x_1$.

In both cases, it is a geodesic fibration*, i.e., the fibers are geodesic 3-tori inside the flat 4-torus.*

Proof. We refer to [30] for the all the details of the proof, and give the main ideas in this section. We first note that the cube complex dual to the decomposition of the 4-tori into cubes is isomorphic to the original decomposition.

We start from (i). Each of the small cusps corresponds to a 4-torus T that is constructed from the inherited colouring on a 4-cube. In this case, the inherited 4-colouring is as in Figure 1.16-(right): each pair of opposite facets shares one colour. The fibration on T is induced by the inherited state and set of moves that are the restriction of the one of P^5. It is simple to note that, by construction, the system of moves is the standard one, and the state is a balanced state. With this choice, the fibration on the torus is simply the diagonal fibration $f(x_1,x_2,x_3,x_4)=x_1+x_2+x_3+x_4$.

The case (ii) is more complicated, since the large boundary tori are adjacent to the bad squares. We therefore need to be more careful, since those are touched by our subdivision into prisms. Let T be one of the large boundary tori, then T is produced by the colouring of the 4-cube in which each facet has a different colour, as in Figure 1.16-(left). As in the previous case, the fibration on T is induced by the inherited state and a set of moves that are the restrictions of those of P^5. The set of moves on the 4-cube consists of 4 pairs of facets like in the previous case, with one key difference: one pair consists of opposite facets, while the other three pairs consist of adjacent facets. The state has opposite statuses on the first pair, and coinciding statuses on each of the other three pairs. The bad 2-squares that separate the pairs of adjacent facets are those contained in the bad ridges of P^5.

As a consequence of this, in the orientation of the edges of the dual $4\times4\times4\times4$ cube complex, there is a direction in which all edges are coherent, and point to the same

direction. This is the direction associated to the pair of opposite facets that belong to the same move, and we will call it the *preferred direction*. Furthermore, the orientation of all the other edges is invariant under translations along the preferred direction.

By looking at a $4 \times 4 \times 4$ cube orthogonal to the preferred direction, after having subdivided all the bad cubes into prisms, one could construct a fiber for the fibration. The fiber could be a complicated 3-dimensional object, and is union of many 3-dimensional polyhedra. However, since there is the preferred direction where all arrows point the same way, all those polyhedra will be transverse to this direction. The fibration is therefore isotopic to the projection along the preferred direction, as desired. □

Chapter 3

Hyperbolic Groups

In this chapter we introduce the concept of hyperbolic groups, and prove two corollaries of Theorem 19, answering two long-standing open questions in geometric group theory.

The concept of hyperbolic groups was introduced first by Gromov in his influential paper [27], and has provoked a paradigm shift in the study of groups, bringing geometric ideas to the forefront. For a short introduction to the topic, we suggest [7] and [54]; for a more extensive description, we recommend [13] and [19].

3.1 Groups as metric spaces

Any finitely generated group G can be seen as a metric space, in a very natural way.

Let T be a finite set of generators, and take $S = T \cup T^{-1}$ in order to have a finite symmetric set of generators. Starting from a group G and a symmetric set of generators S, we can build a graph $\Gamma = \mathrm{Cay}(G, S)$ called the *Cayley graph* of the pair (G, S). The vertices of Γ are the elements of G. There is an edge between two vertices $g, h \in G$ if it exists a generator $s \in S$ such that $g = hs$. We put a metric on G by setting the length of any edge of Γ to be equal to 1, and setting the distance between two vertices to be the length of a shortest path connecting those two vertices. Some examples of Cayley graphs are shown in Figures 3.1, 3.2 and 3.3.

Remark 39. Different sets of generators can produce Cayley graphs of the same group that are not isometric. Two examples for the group $\mathbb{Z}$ are shown in Figure 3.1.

However, any two Cayley graphs of the same group are related by a less restrictive equivalence. For this, we introduce the following definition.

Definition 40. Let (X, d_X) and (Y, d_Y) be metric spaces. A function $f\colon X \to Y$ is said to be a *quasi-isometric embedding* if there are numbers $K, C > 0$ such that

$$\frac{1}{K} \cdot d_X(a, b) - C \leq d_Y(f(a), f(b)) \leq K \cdot d_X(a, b) + C$$

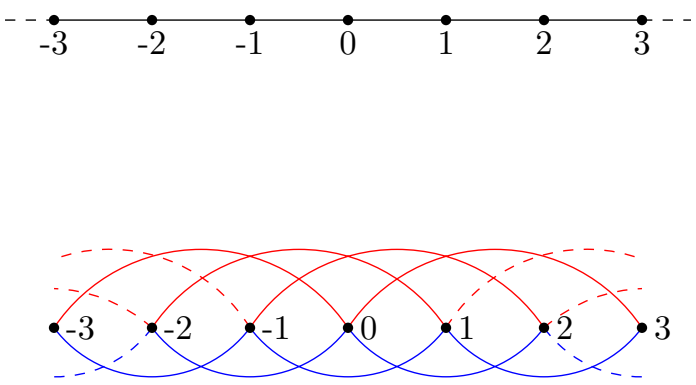

Figure 3.1: Two Cayley graphs for the group $\mathbb{Z}$. In the top, we have chosen $S = \{\pm 1\}$, while in the picture on the bottom $S = \{\pm 2, \pm 3\}$. While their topological properties are very different, they look similar if seen from far away: "they both keep going in two opposite directions".

for all $a, b \in X$. If, in addition, there is a number $R > 0$ such that for every point $y \in Y$ there is $x \in X$ such that $d_Y(y, f(x)) < R$, the function is said to be a *quasi-isometry*. Two spaces are said to be *quasi-isometric* if there is a quasi-isometry from one to the other.

One can verify that the composition of two quasi-isometries is always a quasi-isometry. Moreover, if $f\colon X \to Y$ is a quasi-isometry, then there exists a quasi-isometry $g\colon Y \to X$. In particular, quasi-isometries act as an equivalence relation in the class of metric spaces.

If S and T are two different finite generating sets for G, by carefully bounding the number of generators needed to represent an element of one system with element of the other, one can prove the following proposition.

Proposition 41. *Let G be a group, and let S and T be two finite generating sets for G. Then the identity $G \to G$ is a quasi isometry, if seen as a map between the vertices of the Cayley graphs* $\mathrm{Cay}(G, S) \to \mathrm{Cay}(G, T)$.

For this reason, we will sometimes avoid to specify the set of generators, and simply write $\mathrm{Cay}(G)$, meaning the class of quasi-isometry of any Cayley graph of G.

The following theorem, due to Schwarz [57] and Milnor [44] is often called the Fundamental Theorem of geometric group theory, as it relates groups to properties of the spaces on which they act geometrically.

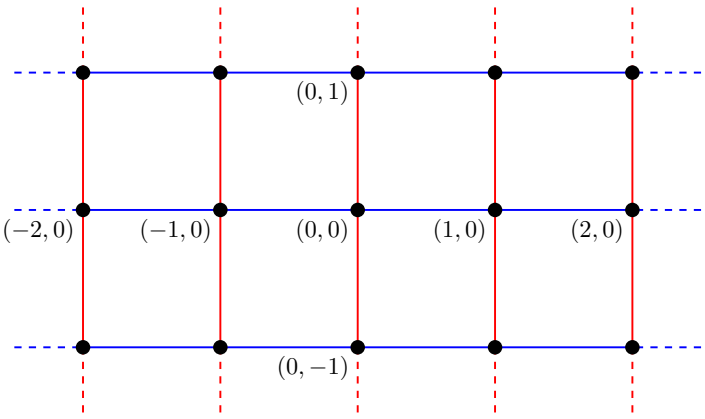

Figure 3.2: The Cayley graph of the group $\mathbb{Z}^2$ with respects to the set of generators $\{(\pm 1, 0), (0, \pm 1)\}$. It is quasi-isometric to the Euclidean plane $\mathbb{R}^2$.

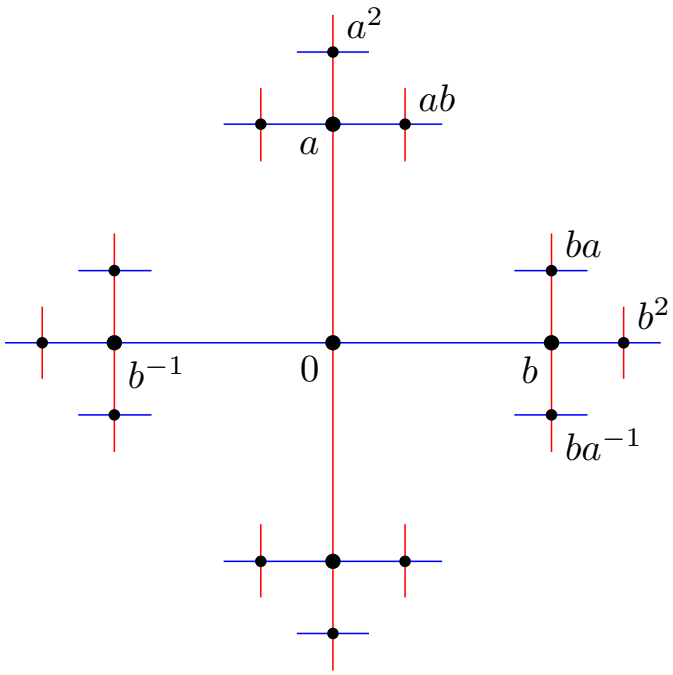

Figure 3.3: The Cayley graph of the free group with two generators $F_2 =< a, b >$, with respects to the set of generators $\{a, b\}$ is a 4-valent tree.

Theorem 42 (Schwarz-Milnor Lemma)**.** *Let X be a proper geodesic metric space X, and suppose that a group G acts properly, cocompactly and by isometries on X. Then there is a finite generating set S for G such that for all $x \in X$ the orbit map*

$$\begin{array}{ccc} \mathrm{Cay}(G,S) & \longrightarrow & X \\ g & \longmapsto & g \cdot x \end{array}$$

is a quasi-isometry.

From now on, we are going to refer to a properly discontinous, cocompact action by isometries of a group G on a metric space X as a *geometric* action.

3.2 Hyperbolic groups

We now introduce the notion of hyperbolic groups, which first appeared in Gromov's famous essay [27]. We start with the following example:

Example 43. If G and H are the fundamental groups of two compact hyperbolic manifolds of the same dimension d, then by Theorem 42 they are both quasi-isometric to the hyperbolic space $\mathbb{H}^d$ and hence to each other.

Inspired by this, we wish to define a concept of hyperbolicity for metric spaces, and then for groups. We start from metric spaces. Here we associate hyperbolicity to having "thin" triangles, such as in Figure 3.4.

Definition 44. Let $\delta \geq 0$ be a real number. A geodesic metric space is said to be *δ-hyperbolic* if for every geodesic triangle xyz, each of the sides is contained in a δ-neighbourhood of the other two sides. A geodesic metric space is said to be *(Gromov)-hyperbolic* if it is δ-hyperbolic for some δ.

Example 45. The following spaces are examples of hyperbolic spaces:

1. Any bounded space with diameter D is D-hyperbolic;
2. A tree is a 0-hyperbolic space. In fact, any geodesic triangle in a tree is completely contained in any two of its sides;
3. The hyperbolic space $\mathbb{H}^n$ is Gromov-hyperbolic.

Example 46. The Euclidean space $\mathbb{R}^n$ is not hyperbolic for each $n \geq 2$. In fact, we can dilate any triangle by a factor of λ, enlarging it to contradict the condition in the definition for any fixed δ. For the same reason, any space that contains a quasi-isometrically embedded copy of the Euclidean plane $\mathbb{R}^2$ cannot be hyperbolic.

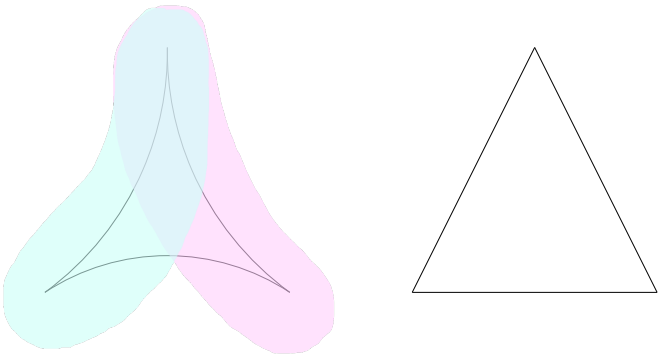

Figure 3.4: On the left, a hyperbolic (thin) triangle, and two neighbourhoods of its sides. On the right, a Eucliden triangle.

A fundamental property of hyperbolic metric spaces is that they satisfy the Morse Lemma [27]. From this crucial fact, it quickly follows that being hyperbolic is a quasi-isometry invariant.

Lemma 47 (Morse Lemma)**.** *Let δ, K, C be fixed positive constants. There is a real number $D = D(\delta, K, C)$ such that for any δ-hyperbolic space X, and any (K, C)-quasi-isometric embedding $f\colon [a, b] \to X$, the image of f is contained in the D-neighbourhood of any geodesic from $f(a)$ to $f(b)$.*

Corollary 48. *If X and Y are quasi-isometric metric spaces, and X is hyperbolic, then also Y is hyperbolic.*

We are now ready to give the main definition.

Definition 49. A group G is said to be *hyperbolic* if it acts geometrically on a hyperbolic metric space X. Equivalently, if G is hyperbolic if $\mathrm{Cay}(G)$ is hyperbolic.

Some examples of hyperbolic groups can be given by adapting Example 45.

Example 50. The following groups are hyperbolic:

1. Finite groups;
2. Free groups, as their Cayley graph is a tree;
3. The fundamental groups of closed hyperbolic n-manifolds, as they act geometrically on $\mathbb{H}^n$.

Any infinite cyclic subgroup of a hyperbolic group G is contained in a maximal virtually cyclic subgroup that contains its normalizer. From this, one could deduce that a hyperbolic group G cannot contain $\mathbb{Z}^2$ as a subgroup. More in general G cannot contain any Baumslag-Solitar subgroup $B(m,n) = \{a, b \mid ba^m b^{-1} = a^n\}$ for $m, n \neq 0$.

Remark 51. The fundamental group of a cusped complete hyperbolic n-manifolds acts by isometries on $\mathbb{H}^n$. However, the action is not cocompact.

3.3 Finiteness properties

A *classifying space* for a group G, also called $K(G,1)$, is an aspherical CW-complex with G as a fundamental group.

Definition 52. A group G is said to be of *type* $\mathcal{F}_n$ if it has a classifying space X with finite n-skeleton. If G is $\mathcal{F}_n$ for each $n \in \mathbb{N}$, we say that G is of *type* $\mathcal{F}_\infty$. Finally, G is said to be of *type* $\mathcal{F}$, or of *finite type*, if it has a finite classifying space.

The property $\mathcal{F}_1$ is equivalent to being finitely generated, while property $\mathcal{F}_2$ is equivalent to be finitely presented. For each integer $n \geq 1$ there is a group of type $\mathcal{F}_n$ but not of type $\mathcal{F}_{n+1}$ [11, 56].

Using the Vietoris–Rips complex it is possible to show that any hyperbolic group is of type $\mathcal{F}_\infty$ [27]. Moreover, one can deduce that a torsion-free hyperbolic group is actually of finite type.

Question 53 (Brady [15])**.** *Let $n \geq 3$ be an integer. Does there exist a hyperbolic group G which has a subgroup $H < G$ that is of type $\mathcal{F}_n$ but not $\mathcal{F}_{n+1}$?*

The case $n = 1$ was solved by Rips in 1982 [53], giving the first example of a *non-coherent* hyperbolic group, i.e., a hyperbolic group with a finitely generated subgroup that is not finitely presented. The topic of coherence of hyperbolic groups has been successively explored in numerous works, see, e.g., [14, 31, 33, 34, 35].

In [15] Brady constructed a hyperbolic group G with a finitely presented subgroup that is not of type $\mathcal{F}_3$, solving the case $n = 2$. It consists on the fundamental group of a ramified covering of a direct product of three graphs. Some other examples were successively constructed by Lodha [42] and Kropholler [38].

By Dehn filling the manifold M^8 constructed in Section 1.10, Llosa Isenrich, Martelli and Py [40] were able to show an example for the case $n = 3$. In particular, they show that the kernel $\ker(f)$ constructed in this thesis is of type $\mathcal{F}_3$ but not $\mathcal{F}_4$. From our construction it is already possible to deduce the kernel is of type $\mathcal{F}_2$ but not $\mathcal{F}_7$.

Using methods from complex hyperbolic geometry, Llosa Isenrich and Py solved the general case [41], showing for each $n \geq 1$ the existence of hyperbolic groups containing subgroups of type $\mathcal{F}_n$ but not $\mathcal{F}_{n+1}$.

In next section we show an example of a subgroup of a hyperbolic group, which is not hyperbolic but has a finite classifying space. This answers a well-known open question, raised in particular by Bestvina [8, Question 1.1], Brady [15, Question 7.2], Bridson [12, Question 4.1], and Jankiewicz, Norin and Wise [31, Section 7].

3.4 Main result

Theorem 54. *There is a hyperbolic group G that contains a subgroup $H < G$ of finite type that is not hyperbolic.*

The proof of this theorem relies on a construction involving the manifold M^5 and the fact it fibers over S^1, as proved in Section 2.8. Let F^4 be the fiber of this fibration. If the manifold M^5 was closed, the groups $H = \pi_1(F^4) = \ker(f_*) < \pi_1(M^5) = G$ would yield the theorem.

Unfortunately, our example has some cusps, so this argument does not work; this is due to the fact that $\pi_1(M^5)$ is not a hyperbolic group. To prove Theorem 54 we are going to perform a Dehn filling construction on M^5, closing its cusps in a way that will be somewhat compatible with the hyperbolic structure. Here is the procedure:

We pick 40 disjoint embedded sections for the 40 cusps of M^5, and we truncate M^5 along them. We get a compact manifold $\overline{M}^5$ such that M^5 is diffeomorphic to the interior of $\overline{M}^5$. The boundary $\partial\overline{M}^5 = X_1 \cup ... \cup X_{40}$ consists of 40 Euclidean 4-tori. By Proposition 38, the restriction to each boundary torus is a geodesic fibration. We can then modify the function $f\colon \overline{M}^5 \to S^1$ via isotopy, so that all restrictions to boundary components are geodesic fibrations. We now define $\overline{F}^4$ to be the fiber of $f\colon \overline{M}^5 \to S^1$: it is a compact 4-manifold whose interior is diffeomorphic to F^4, and whose boundary consists of 3-tori $\partial\overline{F}^4 = T_1 \cup ... \cup T_{136}$. This is due to the fact that the fiber has 4 boundary components in each of the 4-tori corresponding to the 32 small cusps, and one component in the large cusps; as proved in Proposition 38. The total number of boundary components of $\overline{F}$ is therefore $32 \cdot 4 + 8 \cdot 1 = 136$. We select one special boundary component of the fiber $T_i \subset X_i$ for each cusp section X_i, for $i = 1, ..., 40$.

We next fill all boundary tori, in the way that is prescribed by [23, Definition 2.5]. In particular, we cone off the tori T_i by gluing some partial cones $C(X_i, T_i)$ to $\overline{M}^n$. In this way, we obtain a new space $\widehat{M}^n$, in which each leaf of the fibration parallel to T_i is collapsed to a point, and each whole boundary component is replaced by a circle.

More formally, we define

$$C(X_i, T_i) = \frac{X_i \times [0,1]}{\sim}$$

where $(t,1) \sim (t',1)$ if and only if $\tilde{f}(t) = \tilde{f}(t')$, and the function $\tilde{f}$ is defined differently in the two cases of small and large cusps. When the cusp is large we define $\tilde{f} = f$. In small cusps, since the fibration wraps 4 times around the cusps, we replace the map f as described in Proposition 38 with the map $\tilde{f}(x_1, x_2, x_3, x_4) = \frac{1}{4}(x_1 + x_2 + x_3 + x_4)$.

To build the manifold $\widehat{M}^5$, we glue each of the $C(X_i, T_i)$ to the corresponding boundary component $X_i \subset \overline{M}^5$ along its boundary $X_i \times \{0\} = \partial C(X_i, T_i)$.

Remark 55. The space $\widehat{M}^5$ is not a manifold, but just a pseudo-manifold. There is a singular set $S \subset \widehat{M}^5$, consisting of circles, such that $M^5 = \widehat{M}^5 \setminus S$.

The aim of this construction is to be able to use the following theorem:

Theorem 56 ([23], Theorem 2.7)**.** *If all geodesics in the tori T_i are longer than 2π, then there is a complete path metric on $\widehat{M}^5$ induced by the hyperbolic metric of $\overline{M}^5$. This metric is locally $CAT(-k)$ for some $k > 0$.*

The only condition we are left to verify is that all geodesics in the tori T_i must be longer than 2π. To ensure that our tori are big enough, we can perform the previously described construction to a finite cover of M^5 instead of the original manifold M^5. In particular, thanks to the residual finiteness of $\pi_1(M^5)$ we can find a finite index subgroup of $\pi \triangleleft \pi_1(M^5)$ such that in the regular finite cover associated to π all boundary components are 4-tori with systole larger than 2π. The fibration f lifts to this finite cover. For simplicity of notation, we continue to call this new cover M^5. We then close the cusps of this new manifold M as prescribed, obtaining a new space that we continue to call $\widehat{M}^5$. We set $G = \pi_1(\widehat{M}^5)$.

Proposition 57. *The space $\widehat{M}^5$ is aspherical. The group G is hyperbolic and torsion-free.*

Proof. To apply Theorem 56, we just need to check that all geodesics in the 3-tori T_i are longer than 2π. This is true, due to the fact that all closed geodesics in the boundary 4-tori X_i are longer than 2π. Then, we deduce that $\widehat{M}^5$ has a locally $CAT(-k)$ complete path metric for some $k > 0$. In particular $\widehat{M}^5$ is aspherical and $G = \pi_1(\widehat{M}^5)$ is hyperbolic and torsion-free. □

We turn our attention to the fibration $f\colon \overline{M}^5 \to S^1$; when we close the cusps, it quotients to a topological fibration $\hat{f}\colon \widehat{M}^5 \to S^1$. The fiber in this case is homeomorphic

to the space $\widehat{F}^4$ that is obtained by coning off each of the 3-torus boundary components of the original fiber $\overline{F}^4$. Looking at the level of fundamental groups, we get a map

$$\hat{f}_*\colon G = \pi_1(\widehat{M}^5) \to \pi_1(S^1) = \mathbb{Z}.$$

We define the subgroup $H < G$ as the fundamental group of the fiber:

$$H = \pi_1(\widehat{F}^4) = \ker \hat{f}_*.$$

Proposition 58. *The group H is of finite type.*

Proof. Since $H = \pi_1(\widehat{F}^4)$, it is sufficient to show that $\widehat{F}^4$ is aspherical. This is true because $\widehat{M}^5$ is aspherical, and it is covered by $\widehat{F}^4 \times \mathbb{R}$. We deduce that $\widehat{F}^4 \times \mathbb{R}$ is aspherical, and therefore also $\widehat{F}^4$ must be aspherical. □

It remains to be proven that H is not hyperbolic. To do that, we first need to show some preliminary facts.

Proposition 59. *The top cohomology group for both $\widehat{M}^5$ and $\widehat{F}^4$ is $\mathbb{Z}$. In short:*

- $H^5(G) = H^5(\widehat{M}^5) = \mathbb{Z}$;
- $H^4(H) = H^4(\widehat{F}^4) = \mathbb{Z}$.

Proof. As in Remark 55, $M^5 = \widehat{M}^5 \setminus S$ where S is the singular set and consists of some circles. Let νS be a closed regular neighbourhood of S. The exact sequence of the pair $(\widehat{M}^5, S)$ is:

$$0 = H^4(S) \to H^5(\widehat{M}^5, S) \to H^5(\widehat{M}^5) \to H^5(S) = 0.$$

We get that $H^5(\widehat{M}^5, S) = H^5(\widehat{M}^5)$. We now excise the interior of νS, obtaining

$$H^5(\widehat{M}^5) = H^5(\widehat{M}^5, S) = H^5(\widehat{M}^5, \nu S) = H^5(\overline{M}^5, \partial\overline{M}^5) = \mathbb{Z}.$$

The proof for $\widehat{F}^4$ is almost identical. In fact, $F^4 = \widehat{F}^4 \setminus T$ where T is the singular set and consists of some points. The exact sequence of the pair $(\widehat{F}^4, T)$ gives the equality $H^4(\widehat{F}^4, T) = H^4(\widehat{F}^4)$, and excising some small open balls B around the points of T we get the chain of equalities

$$H^4(\widehat{F}^4) = H^4(\widehat{F}^4, T) = H^4(\widehat{F}^4, \bar{B}) = H^4(\overline{F}^4, \partial\overline{F}^4) = \mathbb{Z}.$$

The proof is therefore complete. □

Proposition 60. *The group $\mathrm{Out}(H)$ of the outer automorphisms of H is infinite.*

Proof. Let $\alpha \in \pi_1(\widehat{M^5})$ be an element such that its image $f_*(\alpha)$ generates $\pi_1(S^1) = \mathbb{Z}$. We look at the automorphism $\phi_\alpha \in \mathrm{Out}(H)$ that is given by the conjugation by α: $\phi_\alpha(h) = \alpha h \alpha^{-1}$. We will show that ϕ_α is not trivial in $\mathrm{Out}(H)$, and moreover any of its powers ϕ_α^k are non-trivial for each $k \neq 0$. In this way, the element ϕ_α has infinite order, and therefore the group $\mathrm{Out}(H)$ is infinite.

Suppose by contradiction that there is a $k \neq 0$ such that ϕ_α^k is trivial: this means there is an element $\beta \in H$ such that for all elements $h \in H$ the equality $\alpha^k h \alpha^{-k} = \beta h \beta^{-1}$ holds. In particular, we get that $(\beta^{-1}\alpha^k)h = h(\beta^{-1}\alpha^k)^{-1}$ for each $h \in H$. This means that the element $\gamma := \beta^{-1}\alpha^k \neq e$ commutes with every element of H.

Since G is hyperbolic, and γ has infinite order, then $< \gamma >$ has finite index in the centralizer $C(\gamma)$ [13, Corollary III.Γ.3.10]. We deduce that $C(\gamma)$ must be cyclic, due to the fact that it is virtually cyclic and torsion-free. Since $H < C(\gamma)$, as γ commutes with any element of H, we deduce that also H is infinite cyclic; but this contradicts Proposition 59, as $H^4(H) = \mathbb{Z}$. □

We are finally ready to conclude the proof of Theorem 54.

Proposition 61. *The group H is not hyperbolic.*

Proof. Suppose by contradiction that H is hyperbolic. Since $\mathrm{Out}(H)$ is infinite (as shown in Proposition 60), by Rips' theory [10, Corollary 1.3], the group H splits over a cyclic subgroup. As in [10, Definition 3.1], the following three possibilities arise:

(1) $H = A *_{\mathbb{Z}} B$. In this case we get the exact sequence

$$0 = H^3(\mathbb{Z}) \to H^4(H) \to H^4(A) \oplus H^4(B) \to H^4(\mathbb{Z}) = 0.$$

We deduce that $H^4(A) \oplus H^4(B) = H^4(H) = \mathbb{Z}$. However, both A and B are infinite-index subgroups of H, and therefore they are the fundamental group of an infinite cover of $\widehat{F}^4$. Since such 4-dimensional space is aspherical, and it is not compact, we get that $H^4(A) = H^4(B) = 0$, which is a contradiction.

(2) $H = A * B$. We get again $H^4(A) \oplus H^4(B) = H^4(H) = \mathbb{Z}$ and the same conclusions of the previous case.

(3) $H = A_{\mathbb{Z}}$ is a HNN extension. In this case we get the exact sequence

$$0 = H^3(\mathbb{Z}) \to H^4(H) \to H^4(A) \to H^4(\mathbb{Z}) = 0.$$

Similarly to the previous cases we get $H^4(A) = H^4(H) = \mathbb{Z}$, and we can conclude in the same way, as $H^4(A) = 0$ is a contradiction.

The proof is complete. □

Putting together Proposition 57, Proposition 58 and Proposition 61, yields the proof of Theorem 54.

In this thesis we have presented two necessary conditions for a group G to be hyperbolic: it must be of type $\mathcal{F}_\infty$, and it cannot contain any Baumslag-Solitar subgroup $BS(m,n)$. For some classes of groups, these conditions are actually sufficient: some examples are the fundamental groups of 3-manifolds, free-by cyclic groups [16], and more generally the ascending HNN extensions of free groups [46]. However, as a corollary of Theorem 54, we show that is is not true in full generality, answering a well-known open question, raised in particular by Bestvina [8, Question 1.1], Bridson [12, Question 2.22], Drutu and Kapovich [19, Problem 11.129].

Corollary 62. *There is a finite type group H that is not hyperbolic, and does not contain any Baumslag-Solitar subgroup $BS(m,n)$.*

Proof. Consider G, H such as in Theorem 54. The group H cannot contain any Baumslag-Solitar subgroup, as it is contained in the hyperbolic group G. □

Chapter 4

Conclusions

In this chapter, we explore some possible directions for new research related to the topics presented in this thesis. The main inspiration still comes from the questions that motivated Theorem 19, Theorem 54 and Corollary 62.

The first natural question is whether it is possible to understand better the fibration we have built, from a topological point of view. When a hyperbolic 3-manifold fibers over the circle, the fiber is a finite-type surface, and the monodromy is pseudo-Anosov. It would be interesting to understand what happens in dimension 5, at least in some examples.

Problem 63. *Give a description of the fiber for the fibration of M^5. Determine the monodromy map and study its dynamics.*

The manifold M^5 is tessellated into 256 copies of the polytope P^5, and the combinatorics is too complicated for this investigation. In [30], a smaller fibering manifold is built, which is tessellated into just 2 copies of P^5. It arises from the abelian cover associated to the fibration f, quotiented by some isometries. This new manifold is more manageable in computational terms, and we can describe the fiber explicitly and study it using Regina [17]. In particular, we are able to construct a triangulation for its fiber that uses 144 simplices (of maximal dimension). It is possible to simplify such triangulation obtaining some description that use 40 or 36 simplices (however, this way we lose all information on how the fiber is embedded into the 5-dimensional manifold). Despite this, we were not able to determine the monodromy map.

Another very natural direction of research is to find more examples:

Question 64. *Are there closed examples of hyperbolic 5-manifolds that fiber over the circle?*

The machinery presented here only applies to right-angled polytopes. Unfortunately we only know 5-dimensional hyperbolic polytopes that are in the same commensurability class as P_5. Furthermore, as it was already mentioned, there are no compact right-angled hyperbolic polytopes in dimension higher than 4. One interesting option is to try to generalize this theory to Coxeter polytopes, admitting angles of type $\frac{\pi}{n}$ for all $n \in \mathbb{N}$. However all these approaches are still theoretically dimension-limited, since compact hyperbolic Coxeter polytopes cannot exist in dimension higher than 29 [61], and finite volume hyperbolic Coxeter polytopes cannot not exist in dimension higher than 995 [49].

In a similar fashion, we can explore higher dimensions in pursuit of new examples:

Question 65. *Does the manifold M^7 fiber over S^1?*

Question 66. *Does the manifold M^8 admit a perfect Morse function $f : M^8 \to S^1$?*

Proposition 33 in Chapter 2 ensures that the standard system of moves cannot generate a fibration $f : M^7 \to S^1$. A similar argument holds also for M^8 since its cusps are of similar nature. However, in principle, techniques analogous to the ones described in Section 2.8 could be implemented also in these cases. Unfortunately, here the combinatorics is much more complicated, and no substantial progress has been made.

As already mentioned, a celebrated theorem of Agol and Wise states that all closed hyperbolic 3-manifolds have a finite cover that fibers over the circle [1, 62]. It is a natural question whether this happens also in higher dimensions:

Question 67. *Does every complete, finite volume, odd-dimensional hyperbolic n-manifold virtually fiber over S^1?*

As usual, we can generalize this question to include the even-dimensional case:

Question 68. *Is every complete, finite volume hyperbolic n-manifold finitely covered by one that admits a perfect circle-valued Morse function?*

This question was also asked in [6], and no counterexamples seem to be known at the present time. Similarly to what was observed in Chapter 3, a hypothetical closed fibration would have to have a closed, aspherical manifold F as the fiber, and $\mathrm{Out}(\pi_1(F))$ must be infinite. As observed in [4], this is rare among fundamental groups of higher dimensional aspherical manifolds: all known examples above dimension 2 contain $\mathbb{Z}^2$ and thus do not embed in hyperbolic groups.

A promising tool to approach this topic involves a more algebraic direction: Kielak [36] and Fisher [22] established a close connection between homology growth in finite covers and virtual fibering.

Using fast $\mathbb{F}_p$-homology growth in finite covers to obstruct virtual fibering, Avramidi, Okun and Schreve [4] were able to construct the following example.

Theorem 69. *There exists a closed, odd-dimensional, aspherical manifold M with hyperbolic fundamental group that does not virtually fiber over a circle.*

This theorem does not provide a negative answer to Question 67, since the manifold M is not hyperbolic in the usual sense, but only Gromov-hyperbolic.

We finally focus on the examples provided by Theorem 54 and Corollary 62 in Chapter 3. Every finite type subgroup of a hyperbolic group of cohomological dimension 2 is hyperbolic [25]. The cohomological dimensions of the groups H and G in Theorem 54 are 4 and 5. A natural reformulation of the original question could therefore be the following.

Question 70. *Let G be a hyperbolic group of cohomological dimension $n \leq 4$, and let $H < G$ be a finite type subgroup. Is H hyperbolic?*

Topics related to the absence of Baumslag–Solitar subgroups, and other algebraic versions of hyperbolicity, are studied in [24]. Following this paper, we call a group *BS-free* if it contains no Baumslag–Solitar subgroups $BS(m, n)$. As already mentioned, torsion-free hyperbolic groups are BS-free and have finite classifying spaces. A natural reformulation of the question answered by Corollary 62, as formulated in [24], is the following:

Question 71. *Let G be a group with a finite classifying space of dimension $n \leq 3$. If G is BS-free, is it hyperbolic?*

Bibliography

[1] I. Agol, *The virtual Haken conjecture* (with an appendix by I. Agol, D. Groves and J. Manning), Doc. Math. **18** (2013), 1045–1087.

[2] I. Agol – D. Long – A. Reid, *The Bianchi groups are separable on geometrically finite subgroups*, Ann. Math., **153** (2001), 599–621.

[3] I. Agol – M. Stover, *Congruence RFRS towers*, Annales de l'Institut Fourier, **73** (2023), 307–333.

[4] G. Avramidi, B. Okun, K. Schreve, *Homology growth, hyperbolization, and fibering*, `arXiv:2301.06112`

[5] J. Baez, *The octonions*, Bull. Amer. Math. Soc. **39** (2001), 145–205.

[6] L. Battista – B. Martelli, *Hyperbolic 4-manifolds with perfect circle-valued Morse functions*, Trans. Amer. Math. Soc. **375** (2022), 2597-2625

[7] M. Bestvina, *Groups acting on hyperbolic spaces – a survey*, `arXiv:2206.12916`

[8] M. Bestvina, *Questions in geometric group theory*, `https://www.math.utah.edu/ ~bestvina/eprints/questions-updated.pdf`

[9] M. Bestvina – N. Brady, *Morse theory and finiteness properties of groups*, Invent. Math., **129** (1997), 445–470.

[10] M. Bestvina – M. Feighn, *Stable actions of groups on real trees*, Invent. Math. **121** (1995), 287–321.

[11] R. Bieri, *Homological dimension of discrete groups*, Mathematics Department, Queen Mary College, London, 1976, Queen Mary College Mathematics Notes.

[12] M. Bridson, *Problems concerning hyperbolic and CAT(0) groups*, `https://docs.google.com/file/d/0B-tup63120-GVVZqNFlTcEJmMmc/edit`

[13] M. Bridson – A. Haefliger, "Metric Spaces of Non-Positive Curvature" Grundlehren der Math. Wiss., Vol. 319, Springer-Verlag, Heidelberg, 1999.

[14] B. Bowditch – G. Mess, *A 4-dimensional Kleinian group*, Transactions of AMS **14** (1994), 391–405.

[15] N. Brady, *Branched coverings of cubical complexes and subgroups of hyperbolic groups*, J. London Math. Soc. **60** (1999), 461–480.

[16] P. Brinkmann, *Hyperbolic automorphisms of free groups*, Geom. Funct. Anal., **10** (2000), 1071–1089.

[17] B. Burton, R. Budney, W. Pettersson, et al., Regina: Software for low-dimensional topology, `http://regina-normal.github.io/`, 1999–2021.

[18] S. Choi – H. Park, *Multiplicative structure of the cohomology ring of real toric spaces*, Homology, Homotopy and Applications **22** (2020), 97–115.

[19] C. Drutu – M. Kapovich, with an appendix by B. Nica, "Geometric Group Theory," AMS Colloquium publications 63, 2018.

[20] G. Dufour, *Notes on right-angled Coxeter polyhedra in hyperbolic spaces*, Geom Dedicata **147** (2010), 277–282.

[21] B. Everitt – J. Ratcliffe – S. Tschantz, *Right-angled Coxeter polytopes, hyperbolic six-manifolds, and a problem of Siegel*, Math. Ann. **354** (2012), 871–905.

[22] S. P. Fisher, *Improved algebraic fibrings*, `arXiv:2112.00397`.

[23] K. Fujiwara – J. F. Manning, CAT(0) *and* CAT(-1) *fillings of hyperbolic manifolds*, J. Differential Geom., **85** (2010), 229–269.

[24] G. Gardam, D. Kielak, A. Logan, *Algebraically hyperbolic groups*, `arXiv:2112.01331`

[25] S. M. Gersten, *Subgroups of word hyperbolic groups in dimension 2*, J. London Math. Soc. **54** (1996), 261–283.

[26] T. Gosset, *On the regular and semi-regular figures in space of n dimensions*, Messenger Math. **29** (1900), 43-48.

[27] M. Gromov, *Hyperbolic groups*, Essays in group theory, Math. Sci. Res. Inst. Publ. **8**, Springer, New York, (1987), 75–263.

[28] M. W. Hirsch – B. Mazur, "Smoothings of piecewise linear manifolds," Princeton University Press, Princeton, NJ, 1974, Annals of Mathematics Studies, No. 80.

[29] G. Italiano – B. Martelli – M. Migliorini, *Hyperbolic manifolds that fibre algebraically up to dimension 8*, J. Inst. Math. Jussieu, (2022), 1-38.

[30] G. Italiano – B. Martelli – M. Migliorini, *Hyperbolic 5-manifolds that fiber over S^1*, Invent. Math. **231** (2023), 1-38.

[31] K. Jankiewicz – S. Norin – D. T. Wise, *Virtually fibering right-angled Coxeter groups*, J. Inst. Math. Jussieu, **20** (2021), 957–987.

[32] T. Jørgensen, *Compact 3-manifolds of constant negative curvature fibering over the circle*, Ann. of Math. **106** (1977), 61–72.

[33] M. Kapovich, *Non-coherence of arithmetic hyperbolic lattices*, Geometry & Topology **17** (2013), 39–71.

[34] M. Kapovich – L. Potyagailo, *On the absence of Ahlfors' finiteness theorem for Kleinian groups in dimension three*, Topol. Appl. **40** (1991), 83–91.

[35] M. Kapovich – L. Potyagailo – E. Vinberg, *Non-coherence of some non-uniform lattices in $Isom(\mathbb{H}^n)$*, Geometry and Topology Monographs **14** (2000), 335–351.

[36] D. Kielak, *Residually finite rationally-solvable groups and virtual fibring*, J. Amer. Math. Soc. **33**, No.2 (2020), 451–486.

[37] A. Kolpakov – B. Martelli, *Hyperbolic four-manifolds with one cusp*, Geom. & Funct. Anal. **23** (2013), 1903–1933.

[38] R. Kropholler, *Hyperbolic Groups with Finitely Presented Subgroups not of Type F3*, Geom. Dedicata **213** (2021), 589–619, with an Appendix by G. Gardam.

[39] F. Löbell, *Beispiele geschlossener dreidimensionaler Clifford-Kleinische Räume negativer Krümmung*, Bet. Sächs. Akad. Wiss., **83** (1931), 168–174.

[40] C. Llosa Isenrich – B. Martelli – P. Py, *Hyperbolic groups containing subgroups of type F_3 not F_4*, Journal of Differential Geometry (to appear)

[41] C. Llosa Isenrich – P. Py, *Subgroups of hyperbolic groups, finiteness properties and complex hyperbolic lattices*, Invent. Math. (2023), online first.

[42] Y. Lodha, *A hyperbolic group with a finitely presented subgroup that is not of type FP_3*, Geometric and cohomological group theory, London Math. Soc. Lecture Note Ser. **444**, Cambridge Univ. Press, Cambridge, (2018), 67–81.

[43] M. Migliorini, *Bestvina–Brady Morse theory on hyperbolic manifolds*, Tesi di Perfezionamento, Scuola Normale Superiore, ciclo 35, 19-Dec-2023.

[44] J. Milnor, *A note on curvature and fundamental group*, J. Differential Geometry **2** (1968), 1–7.

[45] J. R. Munkres, *Obstructions to the smoothing of piecewise-differentiable homeomorphisms*, Ann. of Math. (2) **72** (1960), 521–554.

[46] J. P. Mutanguha, *The dynamics and geometry of free group endomorphisms*, Adv. Math. **384** (2021), 107714.

[47] V. Nikulin, *On the classification of arithmetic groups generated by reflections in Lobachevsky spaces*, Math. USSR-Izv. **18** (1982), 99–123.

[48] L. Potyagailo – E. Vinberg, *On right-angled reflection groups in hyperbolic spaces*, Comment. Math. Helv. **80** (2005), 63–73.

[49] M. N. Prokhorov *The absence of discrete reflection groups with noncompact fundamental polyhedron of finite volume in Lobachevsky space of large dimension*, Mathematics of the USSR-Izvestiya **28** (1987), 401-412.

[50] J. Ratcliffe – S. Tschantz, *Volumes of integral congruence hyperbolic manifolds*, J. Reine Angew. Math. **488** (1997), 55–78.

[51] J. Ratcliffe – S. Tschantz, *The volume spectrum of hyperbolic 4-manifolds*, Experiment. Math. **9** (2000), 101–125.

[52] J. Ratcliffe – S. Tschantz, *Integral congruence two hyperbolic 5-manifolds*, Geom. Dedicata **107** (2004), 187–209.

[53] E. Rips, *Subgroups of small cancellation groups*, Bull. London Math. Soc. **14**, No. 1(1982), 45–47.

[54] D. Spriano, *Introduction to Hyperbolic Groups*, Advances in Group Theory and Applications **15** (2023), 63-97.

[55] J Stallings, *On fibering certain 3-manifolds*, in 'Topology of 3-manifolds and related topics" (Proc. The Univ. of Georgia Institute, 1961), pages 95–100. Prentice-Hall, Englewood Cliffs, N.J., 1962.

[56] J Stallings, *A finitely presented group whose 3-dimensional integral homology is not finitely generated*, Amer. J. Math. **85** (1963), 541–543.

[57] A. S. Švarc, *A volume invariant of coverings*, Dokl. Akad. Nauk SSSR (N.S.), **105** (1955), 32–34.

[58] W. Thurston, *On the geometry and dynamics of diffeomorphisms of surfaces*, Bull. Amer. Math. Soc. **19** (1988), 417–431.

[59] W. Thurston, *Hyperbolic structures on 3-manifolds II: surface groups and 3-manifolds which fiber over the circle*, `arXiv:9801045`

[60] A. Vesnin, *Three-dimensional hyperbolic manifolds of Löbell type*, Sibirsk. Mat. Zh., **28** (1987), 50–53, Siberian Math. J., **28** (1987), 731–734.

[61] E. Vinberg *Absence of crystallographic groups of reflections in Lobachevskii spaces of large dimension*, Funct. Anal. Its Appl. **15** (1981), 128-130

[62] D. T. Wise, "The structure of groups with a quasi-convex hierarchy", Princeton University Press, 2021.

[63] `http://people.dm.unipi.it/martelli/research.html`